PHILOSOPHICAL TRANSACTIONS OF THE ROYAL SOCIETY A MATHEMATICAL, PHYSICAL & ENGINEERING SCIENCES

On Nonlinear Effects near the Wing-Tips of an Evolving Boundary-Layer Spot

F. T. Smith

Phil. Trans. R. Soc. Lond. A 1992 **340**, 131-165
doi: 10.1098/rsta.1992.0057

On nonlinear effects near the wing-tips of an evolving boundary-layer spot

By F. T. Smith

Department of Mathematics, University College London, Gower Street, London WC1E 6BT, U.K.

A study is made concerning nonlinear effects arising in the free evolution of three-dimensional disturbances in boundary layers, these disturbances having a spot-like character sufficiently far downstream of the initial disturbance. The theory proposed here takes an inviscid initial-value formulation, typically that involving the three-dimensional unsteady Euler equations; such a formulation is felt to offer hope of considerable analytical progress on the nonlinear side, as well as being suggested by some of the available experimental evidence on turbulent spots and by engineering modelling and previous related theory. As the typical disturbance amplitude is increased, nonlinear effects first enter the reckoning of the large-time large-distance behaviour in edge layers near the spot's wing-tips which correspond to caustics in linear theory. This behaviour is associated with the major length scales, proportional to $(\text{time})^{\frac{1}{2}}$ and to (time), in the evolving spot; within the former scale it is interesting that the three-dimensional Euler flow exhibits a triple-deck-like structure; within the latter scale, in contrast, there are additional time-independent scales in operation. Two possible mechanisms I and II are found for nonlinearity to affect the evolution significantly, near a wing-tip. In I, weakly nonlinear effects make themselves felt in the bulk of the wing-tip flow, accompanied by a near-wall layer where full nonlinearity substantially alters the local vorticity. The analysis then leads to a nonlinear amplitude equation which is the second Painlevé transcendent, whose solution properties are well known. In contrast, mechanism II, which is believed to be the more likely case, has its nonlinearity being mostly due to a three-dimensional mean-flow correction that varies relatively slowly. The resulting nonlinear amplitude equation then has a novel form, solutions for which are obtained computationally and analytically. The further repercussions from the two mechanisms are somewhat different, although each one points to a subsequent flooding of nonlinear effects into the middle of the spot. Mechanism I suggests that strong nonlinearity is produced next by relatively high-amplitude disturbances, whereas the favoured mechanism II indicates instead a strongly nonlinear influence on the mean flow next occurring at input amplitudes that are still relatively low. The additional significance of viscous sublayer bursts is also noted, along with comments on comparisons with experiments and direct numerical simulations. Firm comparisons are felt likely to arise for the next stage implied above, where the middle of a typical spot is affected substantially.

1. Introduction

The evolution of a turbulent spot from an initial localized disturbance in an otherwise planar laminar boundary layer is of much interest in terms of both the

Phil. Trans. R. Soc. Lond. A (1992) **340**, 131–165
Printed in Great Britain

fundamental fluid dynamics involved and the applications. Many experimental studies have been made, with fascinating and somewhat varied results, for example on the main arrowhead-shaped part of the spot, on its tail, on the notional speed of the spot, on its spreading rate, and so on.

Prominent among other very interesting features found experimentally appear to be the following. (*a*) Much of the dynamics in a spot resembles closely that in a fully turbulent boundary layer; see papers from Emmons (1951) to Katz *et al.* (1990) and references therein, and below. (*b*) A turbulent spot develops fast, typically from a localized disturbance with large initial amplitude (Glezer *et al.* 1989; Riley & Gad-el-Hak 1985). (*c*) The growth and spreading of the spot probably take place in a domino-like manner, possibly associated with the successive production of hairpin vortices in the flow near the solid surface (Perry *et al.* 1981; Walker 1990; see also Falco 1979; Smith *et al.* 1991). (*d*) The spanwise growth of the spot greatly exceeds the growth normal to the surface (Gad-el-Hak *et al.* 1981; Glezer *et al.* 1989; and see Bandyopadhyay (1983) for observations on the various angles involved). (*e*) The front and the spanwise side edges, or wing-tips, of the spot are notably sharp, as kindly pointed out to the author by Sir James Lighthill (personal communications): see Lighthill (1963, and references therein), Schlichting (1979), and we note here also Glezer *et al.*s (1989) study of interaction between the spot and trailing wave packets especially near the wing-tips (cf. Chambers & Thomas 1983; Wygnanski *et al.* 1979). Several other experimental features of interest are also described in the above papers, as well as in Schubauer & Klebanoff (1956), Head & Bandyopadhyay (1981), Johansson *et al.* (1987), Henningson & Alfredsson (1987), Robinson (1991), and references therein. Again, interesting computations have been performed by Leonard (1981), Bullister & Orszag (1987), Henningson *et al.* (1987), Henningson & Kim (1991), Fasel (1990), Fasel & Konzelmann (1991) for channel flows (mostly) and boundary layers (more recently). Most are confined to temporal simulations only but they seem to reproduce fairly well some of the major experimental findings. Much extra physical insight and understanding have still to be provided, nevertheless.

It seems clear that a strongly nonlinear theory is desirable for this area but as yet there is no substantial effort in that direction, specifically for spot evolution, i.e. the initial-value problem, as far as we know. (For the record, there is a body of interesting work on nonlinear caustics, in acoustics for example, as in early studies by J.-P. Guiraud and more recently by Howe (1967, 1968), Hunter & Keller (1988), Cates & Crighton (1990), and references therein, as kindly noted by Sir James Lighthill.) Our aim here and in the related works (Doorly & Smith 1992; Smith 1991*a*; see also Gaster 1968), as far as possible, is to develop a nonlinear theory and in particular address the experimental findings (*a*)–(*e*) above. Many complex phenomena arise during spot evolution in practice, there is significant dependence on the particular experimental configurations and conditions used, and there are many nonlinear aspects to be explained or explored, but, as we shall see, a large part of the experimental findings above can be described by the theory, taken in conjunction with the study of Smith *et al.* (1990).

On the theoretical front, then, there is good reason to believe that the Euler stage of Smith *et al.* (1990), Smith & Burggraf (1985) is coming close, or at least the closest of any rational theory for high Reynolds numbers (*Re*), to describing boundary-layer turbulence in a systematic fashion. Support for that belief is provided in the two last-named papers and also by the more empirical modelling of Walker (1990); see also Smith *et al.* (1991), Hoyle *et al.* (1991), Peridier *et al.* (1991*a*, *b*). The local flow within

PHILOSOPHICAL TRANSACTIONS OF THE ROYAL SOCIETY A MATHEMATICAL, PHYSICAL & ENGINEERING SCIENCES

the boundary layer is controlled predominantly by the three-dimensional (3D) unsteady nonlinear Euler equations, according to the above description/model, apart from interludes, however brief, when eruption of the otherwise thin viscous sublayer occurs near the surface and injects a substantial burst of localized vorticity into the Euler flow (see also below). In consequence, it seems not unreasonable to tackle the spot-evolution problem theoretically first by means of the same Euler-stage nonlinear approach, but set as a nonlinear 3D initial-value problem for a localized input disturbance (rather than a fixed-frequency problem, for example). That indeed is the current concern.

Further, the present article considers nonlinear effects acting near the wing-tips or side edges of a spot, since the earlier linear theory of Doorly & Smith (1992) suggests that that is where nonlinearity may appear first naturally as the typical input amplitude is increased (possible alternatives being resonant interactions, vortex/wave interactions, unsteady or nonlinear critical-layer effects). This also has possible connections with the experimental finding (*e*) above. The linear theory just mentioned, in which the initial-value problem can be solved in exact form for some contexts, shows the emergence of a number of distinct zones downstream at comparatively large times, the two main length scales induced being proportional to the scaled time and to its square root. The maximum amplitude, however, is produced in a relatively thin region near the wing-tip of such a linear spot. That property, along with the near-neutrality of the linear-spot behaviour at large times and distances, motivates the present study of nonlinear wing-tip effects. Moreover, these effects are found to lead on subsequently to other cases, corresponding to further increases in the input amplitudes, where nonlinearity can flood into the middle portion of the spot as well.

Certain interesting features arise in the study of 3D nonlinear wing-tip flow. The motion there becomes multi-structured at large times and distances (see §2 below) and it is perhaps surprising to find that the solution of the 3D Euler equations can acquire a 3D triple-deck form, in the square-root scale mentioned above. The downstream motion then develops in one of two ways I or II. The first way (I) exhibits a weakly nonlinear bulk but supplemented by strongly nonlinear near-wall and critical layers (see §§3–5). As a result the mean-flow correction in the bulk becomes singular near the wall, as well as exhibiting a logarithmic dependence and some degree of indeterminacy in the displacement. The near-wall singularity is due to the vanishing of the mean flow itself (which has a linear velocity profile) there, while the indeterminacy is associated with the unknown wall-layer vorticity and possibly with vortex stretching at earlier times. In passing we observe that even in the 2D analogue (Smith & Burggraf 1985) some arbitrariness in the vorticity may be present but it does not have to be, unlike in the current 3D flow. The 2D case, moreover, can give rise to a Benjamin–Ono equation, yielding nonlinear travelling waves or solitary waves, and dispersive waves, that confirm the two length scales (proportional to time and to its square root) referred to previously. In the current 3D setting, the amplitude equation for the nonlinear wing-tip solution appears as a solvability condition in effect and is found to be an Airy equation with an additional nonlinear contribution. The second way (II) has the effects due to a 3D mean-flow correction being dominant, with the wall-layer and critical-layer influences diminished in relative terms, and this again produces a nonlinearly modified Airy equation. The nonlinear amplitude equations for both cases I and II in turn lead on to certain significant repercussions regarding nonlinear effects at increased

PHILOSOPHICAL TRANSACTIONS OF THE ROYAL SOCIETY A MATHEMATICAL, PHYSICAL & ENGINEERING SCIENCES

amplitudes, where interesting scales emerge which seem to be physically sensible, for the middle of the nonlinear spot, although the balances involved then are quite different for the two ways I and II just mentioned. This study and the related works also suggest possible new experiments of interest concerning the effects of increased input amplitudes on spot evolution.

The analysis is presented in §§2–6 below, with further comments being given in §7, while the Appendices A and B are concerned with further detailed points. The global Reynolds number Re, based on the airfoil chord and free-stream speed in the aerodynamic context for example, is assumed large, and we address here the 3D nonlinear incompressible régime. The work is aimed eventually at relatively high-amplitude nonlinear responses, as opposed to gradual transition following linear instability for instance (see also comments in Doorly & Smith (1992) and related papers). Hence we begin in §2 with the 3D Euler context as our main concern, as assumed above. There are in fact three major contexts in which the analysis can be couched, as §2 points out. In all three, the viscous sublayer and its eruptions are neglected here, effectively, as a starting point. These eruptions and the ensuing local vortex formations are important in practice, nevertheless, and they are the subject of other recent theoretical studies, by Smith (1988), Hoyle *et al.* (1991), Peridier *et al.* (1991*a*, *b*), as reviewed by Smith (1991*b*), Walker (1991), Smith *et al.* (1991) for example. Not least, they almost certainly play a key part in the domino process mentioned earlier.

The bulk of the flow in a wing-tip layer is discussed in §3, followed by the critical-layer and wall-layer studies in §§4, 5. The properties found are brought together in §6, along with the pressure-displacement interaction laws, to yield the nonlinear amplitude equation. The equation depends on which of the two ways I and II described in the last-but-one paragraph is dominant, although it is felt that generally the second way is more likely to hold in practice; see §6*a*, *b* and the further discussion in §7.

There may be impact also in several other areas, as noted by Doorly & Smith (1992), including ship wakes and compressible boundary layers. Many issues and aspects are left unresolved, of necessity, and some of these are taken up in related papers. Again, we should emphasize that we do not claim uniqueness in the nonlinear spot behaviour proposed for relatively large times and distances: see also §§5 and 7.

2. The nonlinear initial-value problems, and background

There are three main contexts (figure 1) in which the present work on nonlinear initial-value problems can be set. The first concerns the Euler stage (Smith & Burggraf 1985; Smith *et al.* 1990) for large fully nonlinear disturbances, where the unsteady nonlinear 3D incompressible Euler equations apply,

$$u_x + v_y + w_z = 0, \tag{2.1a}$$

$$u_t + uu_x + vu_y + wu_z = -p_x, \tag{2.1b}$$

$$v_t + uv_x + vv_y + wv_z = -p_y, \tag{2.1c}$$

$$w_t + uw_x + vw_y + ww_z = -p_z, \tag{2.1d}$$

throughout the boundary layer, at large global Reynolds number Re. Here the non-dimensional velocity components u, v, w and the corresponding x, y, z cartesian coordinates (streamwise, normal and spanwise, respectively, with an origin shift) are

PHILOSOPHICAL TRANSACTIONS OF THE ROYAL SOCIETY A MATHEMATICAL, PHYSICAL & ENGINEERING SCIENCES

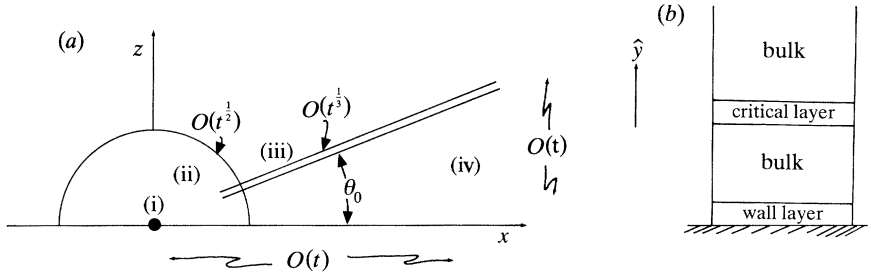

Figure 1. (*a*) Schematic diagram of the flow structure (in xz plan view, upper half only) at large times t, due to the initial disturbance (i), including the $O(t^{\frac{1}{2}})$ elliptic zone (ii) (with three layers in y), the edge layer (iii) near the wing tip, and the $O(t)$ sized zone (iv) further downstream where length scales of $O(1)$ are also induced. This is for the three contexts, and the angle $\theta_0 (\approx 19.47°)$, described in §2. (*b*) The flow structure in the normal direction, within the wing-tip region, for both cases I, II; the wall layers are different for the two cases.

scaled with respect to the local free-stream speed and the typical boundary-layer thickness $O(Re^{-\frac{1}{2}})$, in turn, and similarly for the $O(Re^{-\frac{1}{2}})$ timescale t and the $O(1)$ pressure scale p. The main boundary conditions are

$$(u,v,w,p)\rightarrow\begin{cases}(1,0,0,0) \quad \text{as} \quad y\rightarrow\infty, & (2.2a)\\ (u_0(y),0,0,0) \quad \text{as} \quad x^2+z^2\rightarrow\infty, & (2.2b)\\ v=0 \quad \text{at} \quad y=0, & (2.2c)\end{cases}$$

where the conditions (2.2*a*, *b*) are to match with the free stream outside the boundary layer and with the undisturbed boundary-layer profile $u_0(y)$ holding sufficiently far from the initial disturbance, while (2.2*c*) is the tangential-flow constraint at the solid surface. The profile $u_0(y)$ is supposed here to be monotonic, inflexion-free, and $u_0(\infty)=1$, $u_0(0)=0$, $u_0'(0)=\lambda_0>0$, an example being the Blasius profile. The initial disturbance itself is fully nonlinear, so that

$$(u,v,w,p) \text{ is prescribed (for all } x,y,z) \quad \text{at} \quad t=0, \tag{2.3}$$

consistent with (2.1*a–d*). The problem (2.1*a*)–(2.3) is a computational one generally.

The present research focuses on the issue of the possible solution properties (of the nonlinear initial-value problem above, and those below) at large times, and especially far downstream of the initial-disturbance position, given some guidance from the linearized analysis of Doorly & Smith (1992). At large times t two major length scales arise in the plan-view (xz plane), we suggest, one very far downstream at distances $O(t)$ and the other less far downstream, at distances $O(t^{\frac{1}{2}})$. These two scales also occur in the Doorly & Smith work. Here we are concerned mostly with the $O(t^{\frac{1}{2}})$ length scale, since certain significant features are found to arise first there, even though this is felt to be the zone that trails the majority (the $O(t)$ zone) of the spot. Again, see figure 1. An order-of-magnitude argument suggests that, in the $O(t^{\frac{1}{2}})$ zone, the large-time solution of the unsteady Euler problem (2.1*a*)–(2.3) can take on a three-layer form, analogous with the triple-deck structure. The 'lowest' layer has y being small, with

$$[u,v,w,p]\sim[t^{-\frac{1}{2}}\hat{U},t^{-\frac{3}{2}}\hat{V},t^{-\frac{1}{2}}\hat{W},t^{-1}\hat{p}], \quad y=t^{-\frac{1}{2}}\hat{y}, \tag{2.4a}$$

whereas in the 'middle' layer

$$[u,v,w,p]\sim[u_0(y)+t^{-\frac{1}{2}}\hat{A}u_0'(y),\ -t^{-1}\hat{A}_{\hat{X}}\,u_0(y),O(t^{-1}),t^{-1}\hat{p}], \quad y=O(1), \tag{2.4b}$$

and in the 'uppermost' layer in the outer reaches of the boundary layer

$$[u, v, w, p] \sim [1 + t^{-1}\bar{u}_1, t^{-1}\bar{v}_1, t^{-1}\bar{w}_1, t^{-1}\bar{p}], \quad y = t^{\frac{1}{2}}\bar{y}. \tag{2.4c}$$

Here the unknown surface pressure $\hat{p}(\hat{X}, \hat{Z})$ and negative displacement $\hat{A}(\hat{X}, \hat{Z})$ depend only on the scaled coordinates $\hat{X}, \hat{Z}$, defined by

$$(x, z) = t^{\frac{1}{2}}(\hat{X}, \hat{Z}) \tag{2.5}$$

in the present zone. The main resulting governing equations are those for the lowest layer, namely

$$\hat{U}_{\hat{X}} + \hat{V}_{\hat{y}} + \hat{W}_{\hat{Z}} = 0, \tag{2.6a}$$

$$-\tfrac{1}{2}\hat{U} + (\hat{U} - \tfrac{1}{2}\hat{X})\,\hat{U}_{\hat{X}} + (\hat{V} + \tfrac{1}{2}\hat{y})\,\hat{U}_{\hat{y}} + (\hat{W} - \tfrac{1}{2}\hat{Z})\,\hat{U}_{\hat{Z}} = -\hat{p}_{\hat{X}}, \tag{2.6b}$$

$$-\tfrac{1}{2}\hat{W} + (\hat{U} - \tfrac{1}{2}\hat{X})\,\hat{W}_{\hat{X}} + (\hat{V} + \tfrac{1}{2}\hat{y})\,\hat{W}_{\hat{y}} + (\hat{W} - \tfrac{1}{2}\hat{Z})\,\hat{W}_{\hat{Z}} = -\hat{p}_{\hat{Z}}, \tag{2.6c}$$

from (2.1*a*, *b*, *d*), (2.4*a*), (2.5), with (2.1*c*) confirming that $\partial\hat{p}/\partial\hat{y}$ must be zero; the main boundary conditions are

$$\hat{V} = 0 \quad \text{at} \quad \hat{y} = 0, \tag{2.6d}$$

$$\hat{U} \sim \hat{y} + \hat{A}(\hat{X}, \hat{Z}), \hat{W} \to 0, \quad \text{as} \quad \hat{y} \to \infty, \tag{2.6e}$$

from (2.2*c*) and matching between the expansions (2.4*a*, *b*) respectively, with λ_0 normalized to unity; and the unknown displacement effect present in (2.6*e*) is related to the unknown surface pressure via the double Cauchy–Hilbert integral

$$\hat{p}(\hat{X}, \hat{Z}) = -\frac{1}{2\pi}\int_{-\infty}^{\infty}\int_{-\infty}^{\infty} \frac{\hat{A}_{\xi\xi}(\xi, \phi)\,\mathrm{d}\xi\,\mathrm{d}\phi}{[(\hat{X} - \xi)^2 + (\hat{Z} - \phi)^2]^{\frac{1}{2}}}, \tag{2.7}$$

because of the potential-flow properties induced by (2.4*c*) with (2.1*a–d*) and the matching with (2.4*b*). An alternative formulation for this pressure–displacement interaction is in terms of the pressure in the outermost layer, satisfying

$$(\partial_{\hat{X}}^2 + \partial_{\bar{y}}^2 + \partial_{\hat{Z}}^2)\,\bar{p} = 0, \tag{2.8a}$$

$$\bar{p} \to \hat{p}(\hat{X}, \hat{Z}), \quad \bar{p}_{\bar{y}} \to \hat{A}_{\hat{X}\hat{X}}(\hat{X}, \hat{Z}), \quad \text{as} \quad \bar{y} \to 0+, \tag{2.8b}$$

$$\bar{p} \to 0 \quad \text{in the farfield}, \tag{2.8c}$$

in view of (2.4*b*, *c*), (2.2*a*). Hence we are left with the task of solving the nonlinear, similarity, inviscid-boundary-layer-like system (2.6*a–e*), subject to the interaction law (2.7) or (2.8*a–c*), for the $O(t^{\frac{1}{2}})$ zone properties.

In general the task is still a computational one, and the problem remains elliptic, although probably simpler than the original Euler-equation problem. The work in the following sections considers the possible behaviour of solutions of (2.6), with (2.7) or (2.8), relatively far downstream where $\hat{X}$ is large and positive, $\hat{Z}$ is also large typically, and certain distinctive physical features first emerge. In particular, we examine the flow response near the spot's wing-tips in two 'edge layers', where nonlinear effects can be concentrated (figure 1), these layers lying in the directions given by $\hat{Z} \sim \pm\mu\hat{X}$ say where μ is a positive constant, as indicated by the Doorly & Smith (1992) findings. Thus for $|\hat{Z}| < \mu\hat{X}$, i.e. the entire region between the two edge layers, the flow properties become linear far downstream as in the last paper, and similarly outside where $|\hat{Z}| > \hat{\mu}\hat{X}$, but nonlinear properties hold inside the edge layer where

$$\hat{Z} - \mu\hat{X} = \hat{X}^{-\frac{1}{3}}\eta, \quad \text{with} \quad \eta \quad \text{of} \quad O(1), \tag{2.9}$$

and likewise for the other edge layer near $\hat{Z} = -\mu\hat{X}$. The plan-view scaling in (2.9) is inferred from the last paper, as are the major normal scaling

$$\hat{y} = \hat{X}s, \quad \text{with } s \text{ of } O(1), \tag{2.10}$$

and the expansion of the negative displacement,

$$\hat{A} = \hat{X}^{m-1}(EA_0(\eta) + \text{c.c.}) + \ldots, \tag{2.11a}$$

with

$$E \equiv \exp\left[\mathrm{i}(b_1\hat{X}^2 + \lambda\hat{X}^{\frac{2}{3}}\eta)\right], \tag{2.11b}$$

after some working. The power m is fixed below, while b_1, λ are constants, and c.c. (or, later on, an asterisk) denotes the complex conjugate. If the value of m is sufficiently small or negative (2.11*a*) leads to linear behaviour in the edge layer, as in the last paper, but as m is increased a crucial stage is reached at which nonlinear dynamics first affect the leading-order displacement term A_0. Order-of-magnitude reasoning establishes that crucial value to be when either

$$m = \tfrac{4}{3} \quad \text{or} \quad m = 1, \tag{2.11c, d}$$

and we concentrate first in detail on (2.11*c*) in the following sections, before addressing (2.11*d*), in §6*b*, using similar working. The former seems the more obvious case at first. For, with (2.10), (2.11*a*), the velocity $\hat{U}$ is equal to $\hat{X}s$ with an $O(\hat{X}^{m-1})$ correction, due to (2.6*e*), and so the relative effect of the typical amplitude-squared nonlinearity is of the order $\hat{X}^{2m-4}$. This is to be compared with the relative effect in (2.11*b*), of order $\hat{X}^{-\frac{4}{3}}$. The two effects are comparable when $2m-4 = -\frac{4}{3}$, yielding (2.11*c*). (The alternative reasoning connected with (2.11*d*) is given in §6*b* below.) So (2.11*a*–*c*) form the basis for the nonlinear theory starting in the next section, with the transformations

$$\partial_{\hat{X}} \to \partial_{\hat{X}} - (\mu\hat{X}^{\frac{1}{3}} - \tfrac{1}{3}\eta\hat{X}^{-1})\,\partial_\eta - \hat{X}^{-1}s\,\partial_s \tag{2.12a}$$

$$\partial_{\hat{Z}} \to \hat{X}^{\frac{1}{3}}\partial_\eta, \quad \partial_{\hat{y}} \to \hat{X}^{-1}\partial_s \tag{2.12b, c}$$

and

$$E_{\hat{X}} = (2b_1\hat{X} + \tfrac{2}{3}\lambda\hat{X}^{-\frac{1}{3}}\eta)\,\mathrm{i}E, \quad E_\eta = \lambda\hat{X}^{\frac{2}{3}}\mathrm{i}E, \tag{2.12d, e}$$

from above. In addition, two other $\hat{y}$ scalings can be identified at large $\hat{X}$, one for a near-wall sublayer and the other for a critical layer in effect, and these are studied in §§4, 5. Finally here, the constant μ is equal to $8^{-\frac{1}{2}}$, corresponding to the wake half-angle of $\arcsin\frac{1}{3} = 19.47°$ as in Doorly & Smith (1992), in view of the linearity holding outside and in-between the two edge layers.

Before moving on to the large-distance analysis in §§3–6, we should mention the second and third contexts of interest, further to the first one in (2.1*a*)–(2.3). The second context concerns relatively long-scale disturbances to the boundary-layer motion. These may be viewed as a sub-case in the first context above, with the scalings, for large length factors L,

$$[u, v, w, p] \sim \begin{cases} [L^{-1}, L^{-3}, L^{-1}, L^{-2}], & (2.13a) \\ [u_0(y) + O(L^{-1}), L^{-2}, L^{-2}, L^{-2}], & (2.13b) \\ [1, 0, 0, 0] + O(L^{-2}), & (2.13c) \end{cases}$$

$$[x, z, t] \sim [L, L, L^2], \tag{2.13d}$$

applying for three distinct layers in the normal direction,

$$y \sim L^{-1},\ 1,\ L, \quad \text{in turn.} \tag{2.14a–c}$$

The reasoning is equivalent to that for 3D triple-deck theory (see also above), applied in the present inviscid setting again but now holding for all scaled time. From substitution into (2.1*a–d*), (2.2*a–c*), the resulting governing equations to be addressed are thin-layer versions of (2.1*a–d*), namely with (2.1*a*, *b*, *d*) staying intact but (2.1*c*) replaced by

$$p_y = 0, \quad \text{implying} \quad p = p(x, z, t). \tag{2.15a}$$

Moreover, the boundary conditions become

$$u \sim y + A, \quad w \to 0, \quad \text{as} \quad y \to \infty, \tag{2.15b}$$

$$(u, v, w, p) \to (y, 0, 0, 0) \quad \text{as} \quad x^2 + z^2 \to \infty, \tag{2.15c}$$

along with (2.2*c*), and the unknown pressure and displacement $(-A)$ interact through the outer potential-flow description

$$(\partial_x^2 + \partial_{\bar{y}}^2 + \partial_z^2)\,\bar{p} = 0, \tag{2.15d}$$

$$\bar{p} \to p, \quad \bar{p}_{\bar{y}} \to A_{xx}, \quad \text{as} \quad \bar{y} \to 0+ \tag{2.15e}$$

(or the counterpart of (2.7)), stemming from (2.13*c*). The nonlinear inviscid thin-layer problem is therefore set by (2.1*a*, *b*, *d*), (2.15*a–e*). An apparently self-consistent candidate for the large-time response here, however, is again given by (2.6), with (2.7) or (2.8), since the asymptotes (2.4*a*), (2.5) also tie in exactly with the current context of (2.13*a*)–(2.15*e*) (in a sense, L in (2.13) replaces $t^{\frac{1}{3}}$ in (2.4)). Hence, in turn, the large-distance description of edge layers based on (2.9)–(2.11*c*) also applies to this second context. The third context to note is that of 3D triple-deck theory, where the controlling equations are as for the second context above but with the viscous contributions $\partial^2 u/\partial y^2$, $\partial^2 w/\partial y^2$ added to the right-hand sides of (2.1*b*, *d*) respectively, along with (2.15*a–e*). This occurs if L in (2.13*a*) ff. becomes of the order $Re^{\frac{1}{8}}$, effectively. A short-length or fast-time scaling in this viscous-inviscid context as in Doorly & Smith (1992) then reinstates the inviscid thin-layer version of the second context, however; cf. the finite-time singularity described by Smith (1988), Hoyle *et al.* (1991), Peridier *et al.* (1991*a*, *b*) and Hoyle (1991). In consequence, the large-time large-distance account proposed in (2.6*a–e*), (2.7) (or (2.8*a–c*)), with (2.9)–(2.11*c*), appears to have some relevance to all three contexts, as far as the $O(t^{\frac{1}{3}})$ downstream zone is concerned, although it should be added that the $O(t)$ zones further downstream are case-dependent, and our main interest overall lies in the highest-amplitude case encountered in the first context.

3. Main features in the bulk of the flow

The expansion of the flow solution at relatively large distances $\hat{X} \gg 1$ in the edge layer astride $\hat{Z} = \mu\hat{X}$ is inferred from §2 and takes the underlying form

$$\hat{U} = \hat{X}s + \hat{X}^{\frac{1}{3}}(Eu_0 + E^{-1}u_0^*)\,\kappa + \ldots + \hat{X}^{-\frac{1}{3}}(E^2u_{12}\kappa^2 + Eu_{11}\kappa + u_{10} + E^{-1}u_{11}^*\kappa + E^{-2}u_{12}^*\kappa^2) + \ldots + \hat{X}^{-1}(E^3u_{23}\kappa^3 + \ldots + Eu_{21}\kappa + \ldots) + \ldots, \tag{3.1a}$$

$$\hat{V} = \hat{X}^{\frac{7}{3}}(Ev_0 + E^{-1}v_0^*)\,\kappa + \ldots + \hat{X}^{\frac{5}{3}}(E^2v_{12}\kappa^2 + \ldots) + \ldots + \hat{X}(E^3v_{23}\kappa^3 + \ldots) + \ldots, \tag{3.1b}$$

$$\hat{W} = \hat{X}^{\frac{1}{3}}(Ew_0 + E^{-1}w_0^*)\,\kappa + \ldots + \hat{X}^{-\frac{1}{3}}(E^2w_{12}\kappa^2 + \ldots) + \ldots + \hat{X}^{-1}(E^3w_{23}\kappa^3 + \ldots) + \ldots, \tag{3.1c}$$

for the velocity components, and

$$\hat{p} = \hat{X}^{\frac{4}{3}}(Eg_0 + E^{-1}g_0^*)\,\kappa + \ldots + \hat{X}^{\frac{2}{3}}(E^2 g_{12}\kappa^2 + Eg_{11}\kappa + g_{10}\kappa^2 + E^{-1}g_{11}^*\kappa + E^{-2}g_{12}^*\kappa^2) + \ldots + (E^3 g_{23}\kappa^3 + E^2 g_{22}\kappa^2 + Eg_{21}\kappa + \ldots) + \ldots, \quad (3.1d)$$

$$\hat{A} = \hat{X}^{\frac{1}{3}}(EA_0 + E^{-1}A_0^*)\,\kappa + \ldots + \hat{X}^{-\frac{1}{3}}(E^2 A_{12}\kappa^2 + \ldots + A_{10} + \ldots) + \ldots + \hat{X}^{-1}(E^3 A_{23}\kappa^3 + \ldots + EA_{21}\kappa + \ldots), \quad (3.1e)$$

for the pressure and displacement respectively. Here $\kappa\,(\equiv \hat{X}^{m-\frac{4}{3}}) = 1$, as suggested by (2.11*c*); the alternative (2.11*d*) giving $\kappa = \hat{X}^{-\frac{1}{3}}$ is deferred until §6*b* below. The unknown velocity coefficients u_n, v_n, w_n depend only on s, η, while g_n, A_n are unknown functions of η alone, with the explicit E-dependence as shown. The arrangement of the powers of E in the terms above is partly due to the nonlinear effects present and partly to the wave-like dependence in E defined in §2. The $O(1)$ coordinates s, η are also defined in §2. The successive determination of the first-order contributions u_0, etc., the second-order contributions u_{12}, u_{11}, u_{10}, etc., and the third-order contributions u_{23}, etc., is addressed below, together with additional terms that arise. Here for the sake of generality we consider first the solution properties of (2.6*a–e*) alone, subject to the large-distance behaviour in (3.1*a–e*), before invoking (in §6 below) the extra features implied by the particular external pressure–displacement relation (2.7) or (2.8*a–c*).

Substitution of (3.1*a–e*) into the large-time equations (2.6*a–c*) yields the successive controlling equations as follows. The balances of *continuity* become:

$$\mathrm{i}Bu_0 + v_{0s} + \mathrm{i}\lambda w_0 = 0, \quad \text{where} \quad B \equiv (2b_1 - \lambda\mu), \quad (3.2a)$$

at first order (E terms only);

$$2\mathrm{i}Bu_{12} + v_{12s} + 2\mathrm{i}\lambda w_{12} = 0, \quad (3.2b)$$

$$\mathrm{i}Bu_{11} + v_{11s} + \mathrm{i}\lambda w_{11} - \mu u_{0\eta} + w_{0\eta} = 0, \quad (3.2c)$$

$$v_{10s} = 0, \quad (3.2d)$$

at second order, from contributions proportional to E^2, E, E^0 in turn; and

$$\mathrm{i}Bu_{21} + v_{21s} + \mathrm{i}\lambda w_{21} + \lambda\eta\mathrm{i}u_0 - \mu u_{11\eta} + w_{11\eta} = 0, \quad (3.2e)$$

$$-\mu u_{10\eta} + v_{20s} + w_{10\eta} = 0, \quad (3.2f)$$

at third order, from the terms proportional to E, E^0 respectively. Likewise, the *streamwise momentum* balances yield, at first order,

$$\mathrm{i}\delta u_0 + v_0 = -\mathrm{i}Bg_0 \quad (3.3a)$$

(where the variable $\delta \equiv Bs - b_1$), followed by the second-order contributions in E^2, E, E^0 in turn,

$$2\mathrm{i}\delta u_{12} + v_{12} + \mathrm{i}Bu_0^2 + v_0 u_{0s} + \mathrm{i}\lambda w_0 u_0 = -2\mathrm{i}Bg_{12}, \quad (3.3b)$$

$$\mathrm{i}\delta u_{11} + v_{11} - \mu s u_{0\eta} = -\mathrm{i}Bg_{11} + \mu g_{0\eta}, \quad (3.3c)$$

$$v_{10} + \{-u_0\,\mathrm{i}Bu_0^* + v_0 u_{0s}^* - w_0\,\mathrm{i}\lambda u_0^*\} + \text{c.c.} = 0, \quad (3.3d)$$

and the third-order terms in E, E^0 give respectively

$$\mathrm{i}\delta u_{21} + v_{21} - \mu s u_{11\eta} + (s-1)\,\lambda\eta\mathrm{i}u_0 + \mathrm{i}B(u_{10}u_0 + u_{12}u_0^*) + v_0 u_{10s} + v_0^* u_{12s} + v_{12}u_{0s}^* + \mathrm{i}\lambda(2w_0^* u_{12} + w_{10}u_0 - w_{12}u_0^*) = -\mathrm{i}Bg_{21} + \mu g_{11\eta} - \mathrm{i}\lambda\eta g_0, \quad (3.3e)$$

$$-\mu s u_{10\eta} + v_{20} + f_1 = \mu g_{10\eta}, \quad (3.3f)$$

with

$$f_1 \equiv \{u_0(-\mathrm{i}Bu_{11}^* - \mu u_{0\eta}^*) - u_{11}\,\mathrm{i}Bu_0^* + v_0\,u_{11s}^* + v_{11}\,u_{0s}^* + w_0(-\mathrm{i}\lambda u_{11}^* + u_{0\eta}^*) - w_{11}\,\mathrm{i}\lambda u_0^*\} + \text{c.c.} \quad (3.3g)$$

Finally here, the *spanwise momentum* equations become, at first order,

$$\mathrm{i}\delta w_0 = -\mathrm{i}\lambda g_0, \quad (3.4a)$$

then at second order, for the contributions in E^2, E, E^0 respectively,

$$2\mathrm{i}\delta w_{12} + \mathrm{i}Bu_0\,w_0 + v_0\,w_{0s} + \mathrm{i}\lambda w_0^2 = -2\mathrm{i}\lambda g_{12}, \quad (3.4b)$$

$$\mathrm{i}\delta w_{11} - \mu s w_{0\eta} = -\mathrm{i}\lambda g_{11} - g_{0\eta}, \quad (3.4c)$$

$$\{-u_0\,\mathrm{i}Bw_0^* + v_0\,w_{0s}^* - w_0\,\mathrm{i}\lambda w_0^*\} + \text{c.c.} = 0, \quad (3.4d)$$

while at third order we have

$$\mathrm{i}\delta w_{21} - \mu s w_{11\eta} + (s-1)\,\lambda\eta\mathrm{i}w_0 + \mathrm{i}B(2u_0^*\,w_{12} + u_{10}\,w_0 - u_{12}\,w_0^*) + v_0\,w_{10s} + v_0^*\,w_{12s} + v_{12}\,w_{0s}^* + \mathrm{i}\lambda(w_{10}\,w_0 + w_{12}\,w_0^*) = -\mathrm{i}\lambda g_{21} - g_{11\eta}, \quad (3.4e)$$

$$-\mu s w_{10\eta} + f_2 = -g_{10\eta}, \quad (3.4f)$$

with

$$f_2 \equiv \{u_0(-\mathrm{i}Bw_{11}^* - \mu w_{0\eta}^*) - u_{11}\,\mathrm{i}Bw_0^* + v_0\,w_{11s}^* + v_{11}\,w_{0s}^* + w_0(-\mathrm{i}\lambda w_{11}^* + w_{0\eta}^*) - w_{11}\,\mathrm{i}\lambda w_0^*\} + \text{c.c.}, \quad (3.4g)$$

from the terms involving E, E^0 in turn. The need to include both of these third-order balances is explained subsequently. The forcing effects present in the higher-order balances above stem either from the linear-based modulation existing in the wave part E of §2, as in all the linear terms with subscript zero in (3.2*c*), (3.3*c*), (3.4*c*) and subscripts zero, 11, in (3.2*e*), (3.3*e*), (3.4*e*), or from nonlinear inertial coupling as in the velocity-squared terms throughout (3.3*b*, *d*–*f*), (3.4*b*, *d*–*f*), apart from the variations of the mean-flow correction apparent in (3.3*f*), (3.4*f*). The solutions are as follows.

At first order, (3.2*a*), (3.3*a*), (3.4*a*) apply subject to the constraints

$$v_0 = 0 \quad \text{at} \quad s = 0, \quad u_0 \to A_0 \quad \text{as} \quad s \to \infty, \quad (3.5)$$

from §2. Hence the fundamental solution is given by

$$w_0 = -\frac{\lambda g_0}{\delta}, \quad v_0 = -BA_0\mathrm{i}s, \quad u_0 = A_0 + \frac{\lambda^2 g_0}{B\delta}, \quad (3.6a\text{–}c)$$

with the resulting 'internal' pressure–displacement relation being

$$A_0 = kg_0, \quad \text{and} \quad k \equiv (B^2+\lambda^2)\,B^{-1}b_1^{-1} \quad (3.6d, e)$$

defines the constant k. The results here and in the remainder of this section hold strictly for $\delta \neq 0$, i.e. for $s \neq B^{-1}b_1$, in view of (3.6*a*, *c*) and a *critical layer* is induced, close to the level $\delta = 0$, which is studied in the next section. Another restriction required is that $s > 0$, because it is found below that a *wall layer* is also induced close to the surface as discussed in §5.

At second order, the second harmonic (E^2) components satisfy (3.2*b*), (3.3*b*),

(3.4*b*), subject to (3.5) but with the subscripts zero replaced by 12. These, coupled with the results in (3.6*a–e*), lead to the velocity solution

$$w_{12} = -\frac{\lambda g_{12}}{\delta} - \left(\frac{b_1 - 2Bs}{2\delta^3}\right)\lambda A_0 g_0 B, \tag{3.7a}$$

$$u_{12} = A_{12} - \frac{1}{2\mathrm{i}B}\left(\frac{a_{12}}{\delta} + \frac{b_{12}}{2\delta^2} + \frac{c_{12}}{3\delta^3}\right), \tag{3.7b}$$

$$v_{12} = -2Bi g_{12} - \mathscr{G}_{12} - 2\mathrm{i}\delta u_{12}, \tag{3.7c}$$

where $a_{12} = -2\mathrm{i}\lambda^2 g_{12}$, $b_{12} = 4BA_0 g_0 \mathrm{i}\lambda^2$, $c_{12} = 3b_1 BA_0 g_0 \mathrm{i}\lambda^2$, $\mathscr{G}_{12} = A_0^2 B\mathrm{i} + A_0 g_0 \mathrm{i}\lambda^2(2BS - b_1)\delta^{-2}$, and the internal pressure–displacement relation between g_{12}, A_{12} is

$$2\mathrm{i}b_1 k g_{12} = 2\mathrm{i}b_1 A_{12} - B\mathrm{i}A_0^2. \tag{3.7d}$$

Next, the extra fundamental terms proportional to E are controlled by (3.2*c*), (3.3*c*), (3.4*c*) and (3.5) again, with subscripts 11 instead of zero, and therefore it is found that

$$w_{11} = -\left(\frac{\lambda g_{11} - \mathrm{i}g_{0\eta}}{\delta}\right) + \mathrm{i}\lambda\mu g_{0\eta}\frac{s}{\delta^2}, \tag{3.8a}$$

$$u_{11} = \frac{\mathrm{i}}{B}\left(\frac{a_{11}}{\delta} + \frac{b_{11}}{2\delta^2}\right) + A_{11}, \tag{3.8b}$$

$$v_{11} = \mu s\left[\frac{\lambda^2 g_{0\eta}}{B\delta} + A_{0\eta}\right] - Bi g_{11} + \mu g_{0\eta} - \mathrm{i}\delta u_{11}, \tag{3.8c}$$

where $a_{11} = -\mathrm{i}\lambda^2 g_{11} - 2\lambda(1 + \mu\lambda B^{-1})g_{0\eta}$, $b_{11} = -2\mu\lambda^2 b_1 B^{-1} g_{0\eta}$.

So the internal relation here, between the pressure and displacement coefficients g_{11}, A_{11}, takes the form

$$\mathrm{i}b_1 k g_{11} = \mathrm{i}b_1 A_{11} + B^{-2}\{4b_1^2\mu + (\mu^2 + 1)(\mu\lambda - 4b_1)\lambda\} g_{0\eta}. \tag{3.8d}$$

In contrast, the mean-flow correction proportional to E^0 remains largely undetermined at this level, apart from the result

$$v_{10} \equiv 0, \tag{3.9}$$

consistent with (3.2*d*). This is because both the forcing terms in curly brackets in the two momentum balances (3.3*d*), (3.4*d*) work out to be identically zero, given the fundamental solution in (3.6*a–c*). The absence of governing equations for u_{10}, w_{10} at this order is directly due to these velocities being independent of the fast variable E, by definition, and instead we have to turn to the higher-order balances just below which control the relatively slow variation of the mean-flow-correction velocities u_{10}, w_{10}. Later, in §6*a*, we find the result that for κ unity g_{10} is also identically zero, which again stems from the relative slowness of the mean-flow variation, specifically in the displacement $-E^0 A_{10}$ when inserted in the pressure–displacement link covered by (2.8*a–c*).

At third order, then, we have both the mean-flow (E^0) and the forced-fundamental (E) responses to consider, in the main. The former, which affect the latter, but not vice-versa, are governed by (3.2*f*), (3.3*f*), (3.4*f*) and the outer constraint is $u_{10} \to A_{10}$ as $s \to \infty$, as expected, but the inner constraint here needs extra consideration, as

does that for the forced fundamentals, for the following reason (see also §6*b* below). The solution for the derivative of the spanwise mean-correction velocity follows from (3.4*f*, *g*) in the form

$$w_{10\eta} = \mu^{-1}s^{-1}[\beta_1\delta^{-1} + \beta_2\delta^{-2} + \beta_3\delta^{-3} + g_{10\eta}], \tag{3.10a}$$

on use of the solutions (3.6*a*–*c*), (3.8*a*–*c*), where

$$\beta_1 = 2\lambda\mu k(g_0 g_0^*)_\eta, \quad \beta_2 = b_1 k(2b_1 + 3\lambda\mu)(g_0 g_0^*)_\eta, \quad \beta_3 = 2b_1^2\lambda\mu k(g_0 g_0^*)_\eta. \tag{3.10b–d}$$

The derivative of the streamwise component may then be obtained from (3.2*f*), (3.3*f*, *g*), for example by differentiation of (3.3*f*) with respect to s and elimination of v_{20} using (3.2*f*), yielding the result

$$\begin{aligned} u_{10\eta} = {} & A_{10\eta} + \mu^{-2}s^{-1}[\beta_1\delta^{-1} + \beta_2\delta^{-2} + \beta_3\delta^{-3} + g_{10\eta}] \\ & - \mu^{-1}b_1^{-1}B[(\alpha_1 - \mu^{-1}\beta_1)\{-\delta^{-1} - b_1^{-1}\mathscr{L}\} + 2(\alpha_2 - \mu^{-1}\beta_2)\{-\tfrac{1}{2}\delta^{-2} + b_1^{-1}\delta^{-1} + b_1^{-2}\mathscr{L}\} \\ & + 3(\alpha_3 - \mu^{-1}\beta_3)\{-\tfrac{1}{3}\delta^{-3} + \tfrac{1}{2}b_1^{-1}\delta^{-2} - b_1^{-2}\delta^{-1} - b_1^{-3}\mathscr{L}\}]. \end{aligned} \tag{3.11a}$$

Here

$$\mathscr{L} \equiv \ln|\delta/(b_1 + \delta)|, \quad \alpha_1 = -2\lambda kB^{-1}(2b_1 + \lambda\mu)(g_0 g_0^*)_\eta, \tag{3.11b, c}$$

$$\alpha_2 = -b_1\lambda kB^{-1}(4b_1 + 3\lambda\mu)(g_0 g_0^*)_\eta, \quad \alpha_3 = -2b_1^2\lambda^2 k\mu B^{-1}(g_0 g_0^*)_\eta, \tag{3.11d, e}$$

and the logarithm $\mathscr{L}$ present in (3.11*a*, *b*) requires that (3.11*a*) should be restricted to positive δ (i.e. $s > B^{-1}b_1$, above the critical layer) at first. The result (3.11*a*) continues to hold below the critical layer, however, provided a critical-layer jump contribution is added to $\mathscr{L}$ or equivalently to A_{10}: see §4 below. More significant, as it turns out, are the induced properties of w_{10}, u_{10} near the surface, as $s \to 0+$, where the singular behaviour

$$u_{10} \sim \chi_{-1}s^{-1} + \chi_L \ln s + O(1), \tag{3.12a}$$

$$w_{10} \sim \hat{\chi}_{-1}s^{-1} + O(1), \tag{3.12b}$$

holds, from (3.10*a*), (3.11*a*), given that $g_{10} \equiv 0$ for κ unity. Here $\chi_{-1}, \chi_L, \hat{\chi}_{-1}$ are given in Appendix A. In addition, v_{20} does not tend to zero as $s \to 0$. It follows from (3.12*a*, *b*) that an extra region or wall layer must be produced, near the surface, to smooth out the singularities in the mean flow; the flow features in this wall layer are addressed in §5. It is found also that the inner constraints on the mean-flow terms above, as $s \to 0$, and hence those (see below) on the forced fundamental terms at this level, rely on the wall-flow properties, and so we return to those constraints in §5. In preparation for that, and for the next section, we observe meanwhile that the forced-fundamental solutions are

$$w_{21} = -\mathrm{i}\delta^{-1}\{-\mathrm{i}\lambda g_{21} - g_{11\eta} - (s-1)\lambda\eta\mathrm{i}w_0 + \mu s w_{11\eta} - \mathscr{N}_{21}\}, \tag{3.13a}$$

$$u_{21} = A_{21} - \mathrm{i}\int_\infty^s \delta^{-1}B_{21}\,\mathrm{d}s, \tag{3.13b}$$

formally, from (3.2*e*), (3.3*e*), (3.4*e*), with $u_{21} \to A_{21}$ at large s; here

$$\mathscr{N}_{21} = \sum_{n=1}^{4} L_n\delta^{-n} - \mathrm{i}\lambda g_0\delta^{-1}(\lambda w_{10} + Bu_{10}) - B\mathrm{i}A_0 s w_{10s}, \tag{3.14a}$$

$$\begin{aligned} B_{21} = \sum_{n=1}^{5} Q_n\delta^{-n} + \overline{\overline{Q}} = {} & \lambda\delta^{-1}\{-\mathrm{i}\lambda g_{21} - g_{11\eta} - (s-1)\lambda\mathrm{i}\eta w_0 \\ & + \mu s w_{11\eta} - \mathscr{N}_{21}\} + w_{11\eta} - \lambda\eta\mathrm{i}(s-1)u_{0s} + \mu s u_{11\eta s} - \mathscr{M}_{21s}, \end{aligned} \tag{3.14b}$$

and, on use of the previous lower-order solutions,

$$\left.\begin{aligned} L_1 &= \tfrac{3}{2}\mathrm{i}\lambda k B^{-1}|g_0|^2 g_0, \quad L_2 = 0, \\ L_3 &= -\tfrac{5}{2}\mathrm{i}\lambda k^2 B^2 b_1 |g_0|^2 g_0, \quad L_4 = -\tfrac{3}{2}\mathrm{i}\lambda k^2 B^2 b_1^2 |g_0|^2 g_0, \end{aligned}\right\} \tag{3.14c}$$

$$\mathscr{M}_{21} = \sum_{n=0}^{4} K_n \delta^{-n} + (\lambda^2 g_0 B^{-1}\delta^{-1} + A_0)\,\mathrm{i}(\lambda w_{10} + B u_{10}) - A_0 B i s u_{10s}, \tag{3.14d}$$

with

$$\left.\begin{aligned} K_0 &= \mathrm{i}BA_0^* A_{12}, \quad K_1 = \mathrm{i}\lambda^2(g_0^* A_{12} + A_0^* g_{12}), \quad K_2 = 0, \\ K_3 &= \tfrac{5}{2}\mathrm{i}\lambda^2 k^2 b_1 B|g_0|^2 g_0, \quad K_4 = \tfrac{3}{2}\mathrm{i}\lambda^2 k^2 b_1^2 B|g_0|^2 g_0, \end{aligned}\right\} \tag{3.14e}$$

and

$$\begin{aligned} \overline{\overline{\mathrm{Q}}} = {} & 2\lambda^2 \mathrm{i} g_0 \delta^{-2}(\lambda w_{10} + B u_{10}) + \lambda B \delta^{-1} \mathrm{i} s k g_0 w_{10s} \\ & - \mathrm{i} g_0 (\lambda^2 B^{-1}\delta^{-1} + k)(\lambda w_{10s} + B u_{10s}) + \mathrm{i} k g_0 B (s u_{10s})_s. \end{aligned} \tag{3.14f}$$

Hence the forced fundamentals in (3.13*a*, *b*) also become singular as $s \to 0$, in the form

$$u_{21} \sim \kappa_{-1} s^{-1} + \kappa_L \ln s + O(1), \tag{3.15a}$$

$$v_{21} \sim (\mathrm{i}b_1 \kappa_L - \hat{\kappa}_L)\ln s + O(1), \quad w_{21} \sim \tilde{\kappa}_{-1} s^{-1} + O(1), \tag{3.15b, c}$$

(see coefficients in Appendix A), in view of the singular mean-flow response in (3.12*a*, *b*) and the appearance of u_{10}, w_{10} in (3.13*a*) ff. It is found also that the presence of logarithmic terms here and in (3.12*a*) requires insertion of a mean-flow term, $\hat{X}^{-\frac{1}{3}} \ln \hat{X} u_{10L}$ say, in $\hat{U}$ in (3.1*a*), along with a forced fundamental $\hat{X} \ln \hat{X} E v_{21L}$ in $\hat{V}$. It is then found that the solution for u_{10L} is simply the displaced form $u_{10L} = A_{10L}$, independent of Y, and that $v_{21L} \propto g_0 A_{10L}$, with A_{10L} to be determined. Matching with the wall layer of §5 below, however, then requires, in effect, the tangential-flow constraint that $g_0 A_{10L} \propto (\mathrm{i}b_1 \kappa_L - \hat{\kappa}_L)$ from (3.15*b*), which fixes the form of A_{10L}. These terms have no substantial influence on the other terms examined here and in the following sections. The main features are the singularities in (3.12*a*, *b*), (3.15*a*–*c*), and these and other aspects are taken up again in §5, after the study of the critical layer immediately below.

4. The critical layer

The critical layer occurs at small δ, in the midst of the bulk flow, with the normal scaling

$$\hat{y} = B^{-1}(b_1 \hat{X} + \hat{X}^{\frac{2}{3}} \Delta) \tag{4.1}$$

holding, where Δ is now $O(1)$ and in effect $\delta \to \hat{X}^{-\frac{1}{3}}\Delta$, for the case $\kappa = 1$ still. The expansions of the flow solution here, as implied by the breakdown of those in §3 at small δ, are

$$\hat{U} = B^{-1} b_1 \hat{X} + \hat{X}^{\frac{2}{3}} \tilde{U}_1 + \hat{X}^{\frac{1}{3}} \tilde{U}_2 + \tilde{U}_3 + \hat{X}^{-\frac{1}{3}}(\tilde{U}_{4L} \ln \hat{X} + \tilde{U}_4) + \ldots, \tag{4.2a}$$

$$\hat{V} = \hat{X}^{\frac{7}{3}} \tilde{V}_1 + \ldots, \tag{4.2b}$$

$$\hat{W} = \hat{X}^{\frac{2}{3}} \tilde{W}_1 + \hat{X}^{\frac{1}{3}} \tilde{W}_2 + \ldots, \tag{4.2c}$$

with $\hat{p}$ remaining as in §3. So the general relative error is now of the order $\hat{X}^{-\frac{1}{3}}$, cf. §3. Also, the transformations

$$\partial_{\hat{X}} \to \partial_{\hat{X}} - (\mu \hat{X}^{\frac{1}{3}} - \tfrac{1}{3}\hat{X}^{-1}\eta)\,\partial_\eta - (b_1 \hat{X}^{-\frac{2}{3}} + \tfrac{2}{3}\hat{X}^{-1}\Delta)\,\partial_\Delta, \tag{4.3a}$$

$$\partial_{\hat{y}} \to B\hat{X}^{-\frac{2}{3}}\partial_\Delta, \quad \partial_{\hat{Z}} \to \hat{X}^{\frac{1}{3}}\partial_\eta \tag{4.3b, c}$$

apply, and there is dependence on the variable

$$F \equiv (b_1 \hat{X}^2 + \hat{X}^{\frac{3}{2}} \lambda \eta) \tag{4.3d}$$

as the fastest scale, in essence through terms E^n, where $E \equiv \exp(\mathrm{i}F)$.

The *continuity* balances resulting from substitution of (4.2) into (2.6a) are therefore

$$\mathscr{L}(\tilde{U}_1, \tilde{V}_1, \tilde{W}_1) = 0 = \mathscr{L}(\tilde{U}_2, \tilde{V}_2, \tilde{W}_2) = \mathscr{L}(\tilde{U}_3, \tilde{V}_3, \tilde{W}_3) - \mu \tilde{U}_{1\eta} + \tilde{W}_{1\eta}$$
$$= \mathscr{L}(\tilde{U}_4, \tilde{V}_4, \tilde{W}_4) - \mu \tilde{U}_{2\eta} + \tilde{W}_{2\eta}, \tag{4.4a–d}$$

where the operator $\mathscr{L}(u, v, w) \equiv B(u_F + v_\Delta) + \lambda w_F$. Likewise, the *streamwise momentum* balances

$$B(\tilde{U}_1 \tilde{U}_{1F} + \tilde{V}_1 \tilde{U}_{1\Delta}) + \lambda \tilde{W}_1 \tilde{U}_{1F} = -\mathrm{i}Eg_0 B + \text{c.c.}, \tag{4.5a}$$

$$B(\tilde{U}_2 \tilde{U}_{1F} + \ldots) - \mu b_1 B^{-1} \tilde{U}_{1\eta} = 0, \tag{4.5b}$$

$$B(\tilde{U}_3 \tilde{U}_{1F} + \ldots) - \mu \tilde{U}_1 \tilde{U}_{1\eta} - \mu b_1 B^{-1} \tilde{U}_{2\eta} + \tilde{W}_1 \tilde{U}_{1\eta} = -\mathrm{i}Eg_{11} B + \mu g_{0\eta} E - 2\mathrm{i}E^2 g_{12} B + \text{c.c.}, \tag{4.5c}$$

$$B(\tilde{U}_4 \tilde{U}_{1F} + \ldots) - \mu(\tilde{U}_2 \tilde{U}_{1\eta} + \tilde{U}_1 \tilde{U}_{2\eta}) - \mu b_1 B^{-1} \tilde{U}_{3\eta} + \tfrac{1}{2}\lambda^2 \mu B_\eta^{-1} \tilde{U}_{1F}$$
$$+ (\tilde{W}_2 \tilde{U}_{1\eta} + \tilde{W}_1 \tilde{U}_{2\eta}) - \tfrac{1}{2}\lambda \mu \tilde{U}_{1F} = 0 \tag{4.5d}$$

are obtained from (2.6b), with analogous equations holding for the *spanwise momentum* balances from (2.6c), and similarly for the $4L$ terms in (4.2a) ff. The critical layer is 'fully nonlinear' in the sense that the dominant inertial operator, in (4.5a), includes the contributions $\tilde{U}_1 \tilde{U}_{1F}$, etc. (see Benney & Bergeron 1969; Haberman 1972; Smith & Bodonyi 1982; Bodonyi *et al.* 1983; Smith *et al.* 1990 and references therein). This is due to the main flow speed in (4.2a) being equal to the effective phase speed present and due to the effective disturbance sizes in (4.2a–c) and earlier in (3.1a–e).

Relatively simple solutions appear to exist, nevertheless, although we should stress that there can still be arbitrariness present through the active vorticity as in the wall-layer behaviour addressed in the next section. With the definitions

$$q_n \equiv B\tilde{U}_n + \lambda \tilde{W}_n, \quad v_n \equiv B\tilde{V}_n, \quad n \geqslant 1, \tag{4.6}$$

introduced, governing equations for q_n, v_n can be derived by adding B times the above streamwise momentum equations to λ times the spanwise ones, and the appropriate boundary conditions stem from matching at large Δ with the bulk-flow solutions of §3 at small δ. A possible solution at leading order is then simply

$$q_1 = \Delta, \quad v_1 = -\mathrm{i}Eg_0(B^2 + \lambda^2) + \text{c.c.}, \tag{4.7}$$

while at second order

$$q_2 = B(EA_0 + \text{c.c.}), \quad v_2 = -BA_0 \Delta \mathrm{i}E + \text{c.c.} \tag{4.8}$$

is a possible form. We are then left with finding q_3, q_4, and so on. The individual velocity components at this stage are given by

$$\tilde{W}_1 = B^{-1} b_1^{-1} k^{-1} \lambda \Delta + h_1(\xi, \eta), \tag{4.9a}$$

$$\tilde{W}_2 = \int [B^{-1} b_1 \mu \tilde{W}_{1\eta} - B(EA_0 + \text{c.c.})\, \tilde{W}_{1F} + B(\mathrm{i}EA_0 + \text{c.c.})\, \Delta \tilde{W}_{1\Delta}] \frac{\mathrm{d}F}{2^{\frac{1}{2}}(\xi - H(F))^{\frac{1}{2}}} + h_2(\xi, \eta), \tag{4.9b}$$

from solving the analogues of (4.5*a*, *b*), where h_1, h_2 are arbitrary functions of η and $\xi = \frac{1}{2}\Delta^2 + H$, apart from the matching requirements at large $|\Delta|$, $H_F = -v_1$, and the integration in (4.9*b*) is at fixed ξ. The solutions for $\tilde{U}_1, \tilde{U}_2$ then follow from (4.6)–(4.8).

The above shows that the irregularities in the solutions of §3 as $\delta \to 0\pm$ (which appear here as $\Delta \to \pm\infty$) are smoothed out satisfactorily inside the nonlinear critical layer. Next we examine higher-order terms also, to verify a similar effect for them. The third-order contributions q_3, v_3 are governed by the combined continuity and momentum equations

$$q_{3F} + v_{3\Delta} = \mu\tilde{U}_{1\eta} - \tilde{W}_{1\eta}, \tag{4.10a}$$

$$\Delta q_{3F} + v_1 q_{3\Delta} + v_3 = -q_2 q_{2F} + B^{-1}\mu b_1 q_{2\eta} - \pi_3 \tag{4.10b}$$

subject to the matching conditions, for $\Delta \to \pm\infty$,

$$q_3 \sim \Delta^{-1}[-2B^{-1}b_1\lambda \mathrm{i} g_{0\eta} E + \text{c.c.} + 2B^2\mu^{-2}k|g_0|^2] + O(\Delta^{-3}), \tag{4.10c}$$

$$v_3 \sim E\{2g_{0\eta}(2b_1\mu - \lambda - \lambda\mu^2) - \mathrm{i}g_{11}kb_1\} + E^2\{-2\mathrm{i}g_{12}b_1 k - \mathrm{i}k^2 g_0^2 B\} + O(\Delta^{-2}), \tag{4.10d}$$

after some manipulation. At fourth order q_4, v_4 are found to satisfy

$$q_{4F} + v_{4\Delta} = \mu\tilde{U}_{2\eta} - \tilde{W}_{2\eta}, \tag{4.11a}$$

$$\Delta q_{4F} + v_1 q_{4\Delta} + v_4 = -(q_2 q_3)_F - v_2 q_{3\Delta} + (\mu\tilde{U}_1 - \tilde{W}_1) q_{2\eta} + B^{-1}\mu b_1 q_{3\eta}, \tag{4.11b}$$

with the matching conditions

$$q_4 \sim \Gamma_0 \ln|\Delta| + \Gamma_1 + \Gamma_2 \Delta^{-2} E + \ldots, \quad v_4 \sim \chi\Delta + o(\Delta^{-1}), \tag{4.11c, d}$$

for $\Delta \to \pm\infty$, again from §3, where

$$\Gamma_0 = 4kB^2\mu^{-2}b_1^{-1}|g_0|^2, \quad \Gamma_1 = B(A_{11}E + A_{12}E^2) + \text{c.c.} + \Gamma_{10}^{\pm}, \tag{4.12a, b}$$

$$\Gamma_2 = -2B^{-2}\lambda\mu b_1^2 g_{0\eta\eta}, \quad \chi = (\mu A_{0\eta} - \mathrm{i}BA_{11})E - 2\mathrm{i}A_{12}BE^2 + \text{c.c.}, \tag{4.12c, d}$$

and $\Gamma_{10}^{\pm}$ are constants. The conditions (4.10*c*, *d*), (4.11*c*, *d*) can be shown to be consistent with the governing equations (4.10*a*, *b*), (4.11*a*, *b*) at large $|\Delta|$. The complete solutions of (4.10*a*–*d*), (4.11*a*–*d*) may be obtained formally in a manner similar to that in (4.9*a*, *b*), the latter being used to evaluate the right-hand side forcing terms in (4.10*a*, *b*), (4.11*a*, *b*). These solutions may be derived by solving for the skewed shears first, e.g. $\tau_3 \equiv \partial q_3/\partial\Delta$ satisfies the simplified equation $\Delta\,\partial\tau_3/\partial F = 2B^{-1}b_1\,\partial\tilde{W}_1/\partial\eta$ at fixed ξ, after which q_3 is obtained from an integration. The results although cumbersome confirm that the required asymptotes are reached at large $|\Delta|$ and the solutions are smooth for Δ of $O(1)$, thus verifying the removal of the singularities obtained in §3. Moreover, the property (4.12*b*), which stems from substitution into the governing equations, indicates that there is no jump associated with the logarithmic term in (3.11*a*, *b*) (or otherwise, as yet), as the critical layer is crossed, except possibly for a constant. The latter in fact adds to the arbitrariness described in the next two sections. Finally here, the logarithmic contributions in (4.2*a*) ff. have

$$\tilde{U}_{4L\eta} \sim 2(\alpha_2 - \mu^{-1}\beta_2)B/(3\mu b_1^3) + O(\Delta^{-2}), \quad \tilde{W}_{4L} = O(\Delta^{-2}), \tag{4.13}$$

at large $|\Delta|$, again matching with the bulk-flow results as required; see also near the end of the previous section. The solution for $\tau_{4L} \equiv \partial q_{4L}/\partial\Delta$ is found to be an arbitrary function of ξ, η which is $o(\Delta^{-3})$ at large $|\Delta|$ and possibly is zero throughout, in which case q_{4L} is equal to B times the $O(1)$ term in (4.13).

5. The wall layer

This extra layer arises because of the singular response $O(s^{-1})$ of the mean-correction velocities in (3.12a, b), cf. §6b below, and is found to play an important role. The thickness of the wall layer for the case $\kappa = 1$ may be deduced from comparison of the basic mean-flow term $\hat{X}s$ in (3.1a) and the correction term $O(\hat{X}^{-\frac{1}{3}}s^{-1})$ due to u_{10}, giving the scaling as $s \sim \hat{X}^{-\frac{2}{3}}$, i.e. $\hat{y} \sim \hat{X}^{\frac{1}{3}}$. The implied expression for the wall-layer flow solution is therefore

$$\hat{U} = \hat{X}^{\frac{1}{3}}\bar{u}_0 + \hat{X}^{-\frac{1}{3}}\ln\hat{X}\bar{u}_{1L} + \hat{X}^{-\frac{1}{3}}\bar{u}_1 + \ldots, \tag{5.1a}$$

$$\hat{V} = \hat{X}^{\frac{5}{3}}\bar{v}_0 + \hat{X}\bar{v}_1 + \ldots, \tag{5.1b}$$

$$\hat{W} = \hat{X}^{\frac{1}{3}}\bar{w}_0 + \hat{X}^{-\frac{1}{3}}\ln\hat{X}\bar{w}_{1L} + \hat{X}^{-\frac{1}{3}}\bar{w}_1 + \ldots, \tag{5.1c}$$

from the behaviours of the bulk-flow components in §3. Here $\hat{y} = \hat{X}^{\frac{1}{3}}Y$ with Y of order unity typically, so that

$$\partial_{\hat{X}} \to \partial_{\hat{X}} - (\mu\hat{X}^{\frac{1}{3}} - \tfrac{1}{3}\hat{X}^{-1}\eta)\,\partial_\eta - \tfrac{1}{3}\hat{X}^{-1}Y\,\partial_Y, \tag{5.2a}$$

$$\partial_{\hat{Z}} \to \hat{X}^{\frac{1}{3}}\partial_\eta, \quad \text{and} \quad \partial_{\hat{y}} \to \hat{X}^{-\frac{1}{3}}\partial_Y. \tag{5.2b, c}$$

There is dependence again on the fast variable $F \equiv (b_1X^2 + X^{\frac{2}{3}}\lambda\eta)$ generally through all the powers of $E = \exp(\mathrm{i}F)$ present, in effect; among the terms shown in (5.1a–c) only $\bar{u}_{1L}, \bar{w}_{1L}$ are independent of F.

At leading order, the governing equations from substitution into (2.6a–c) are

$$B\bar{u}_{0F} + \bar{v}_{0Y} + \lambda\bar{w}_{0F} = 0, \tag{5.3a}$$

$$-b_1\,\bar{u}_{0F} = -Big_0E + \text{c.c.}, \quad -b_1\,\bar{w}_{0F} = -\lambda ig_0E + \text{c.c.}, \tag{5.3b, c}$$

for the continuity and the streamwise and spanwise momentum balances in turn. So the solution has the form

$$\bar{u}_0 = b_1^{-1}B(g_0E + g_0^*E^{-1}) + \overline{\bar{u}}(\eta, Y), \tag{5.4a}$$

$$\bar{v}_0 = -\mathrm{i}b_1^{-1}(B^2 + \lambda^2)\,(g_0E - g_0^*E^{-1})\,Y, \tag{5.4b}$$

$$\bar{w}_0 = b_1^{-1}\lambda(g_0E + g_0^*E^{-1}) + \overline{\bar{w}}(\eta, Y). \tag{5.4c}$$

Here the parts involving E, E^{-1} match as required with the bulk solutions of §3 at small s: see (3.6a–c). The parts $\overline{\bar{u}}, \overline{\bar{w}}$ on the other hand, remain undetermined as yet, apart from the requirement that

$$\overline{\bar{u}} \sim Y + \chi_{-1}Y^{-1}, \quad \overline{\bar{w}} \sim \hat{\chi}_{-1}Y^{-1} \quad \text{as} \quad Y \to \infty \tag{5.4d, e}$$

to merge with (3.1a, c), given (3.12a, b). Further, in the sense that $\overline{\bar{u}}, \overline{\bar{w}}$ represent the *total* mean flow, the general effect here is a *fully nonlinear* one.

To uncover more about the mean flow in the present layer we proceed to higher-order effects. The controlling equations at the next order are found to be

$$B\bar{u}_{1F} + \bar{v}_{1Y} + \lambda\bar{w}_{1F} - \mu\bar{u}_{0\eta} + \bar{w}_{0\eta} = 0, \tag{5.5a}$$

$$-b_1\,\bar{u}_{1F} + B\bar{u}_0\,\bar{u}_{0F} + \bar{v}_0\,\bar{u}_{0Y} + \lambda\bar{w}_0\,\bar{u}_{0F} = -(G1X), \tag{5.5b}$$

$$-b_1\,\bar{w}_{1F} + B\bar{u}_0\,\bar{w}_{0F} + \bar{v}_0\,\bar{w}_{0Y} + \lambda\bar{w}_0\,\bar{w}_{0F} = -(G1Z), \tag{5.5c}$$

where

$$G1X = \{(Big_{11} - \mu g_{0\eta})E + 2Bi E^2 g_{12}\} + \text{c.c.},$$

$$G1Z = \{(\lambda ig_{11} + g_{0\eta})E + 2\lambda i E^2 g_{12}\} + \text{c.c.}$$

These yield the solutions, from the momentum balances (5.5*b*, *c*) (the continuity equation (5.5*a*) is used later),

$$\bar{u}_1 = (\bar{u}_{11} E + \bar{u}_{12} E^2) + \text{c.c.} + \overline{\bar{u}}_1(\eta, Y), \tag{5.6a}$$

$$\bar{w}_1 = (\bar{w}_{11} E + \bar{w}_{12} E^2) + \text{c.c.} + \overline{\bar{w}}_1(\eta, Y), \tag{5.6b}$$

with $\overline{\bar{u}}_1, \overline{\bar{w}}_1$ being further, unknown, mean-flow contributions, while

$$\bar{u}_{11} = b_1^{-2} g_0 \{(B\overline{\bar{u}} + \lambda \overline{\bar{w}}) B - (B^2 + \lambda^2) Y \overline{\bar{u}}_Y\} + B b_1^{-1} g_{11} + \mathrm{i} b_1^{-1} \mu g_{0\eta}, \tag{5.6c}$$

$$\bar{u}_{12} = B b_1^{-1} g_{12} + \tfrac{1}{2} B b_1^{-3} g_0^2 (B^2 + \lambda^2), \tag{5.6d}$$

$$\bar{w}_{11} = b_1^{-1}(\lambda g_{11} - \mathrm{i} g_{0\eta}) + b_1^{-2} g_0 \{(B\overline{\bar{u}} + \lambda \overline{\bar{w}})\lambda - (B^2 + \lambda^2) Y \overline{\bar{w}}_Y\}, \tag{5.6e}$$

$$\bar{w}_{12} = \lambda b_1^{-1} g_{12} + \tfrac{1}{2} \lambda b_1^{-3} g_0^2 (B^2 + \lambda^2). \tag{5.6f}$$

The velocity expressions (5.6*a*, *b*) combined with the asymptotes (5.4*d*, *e*) can be shown to match satisfactorily at large Y with the bulk-flow velocity solutions of §3 at small s. No extra conditions on the total mean flow are found, however, at this level.

At a higher order, the governing equations of §2 yield the momentum balances

$$-b_1 \bar{u}_{2F} + B(\bar{u}_0 \bar{u}_{1F} + \bar{u}_1 \bar{u}_{0F}) + (\bar{v}_1 \bar{u}_{0Y} + \bar{v}_0 \bar{u}_{1Y}) + \lambda(\bar{w}_0 \bar{u}_{1F} + \bar{w}_1 \bar{u}_{0F}) - \mu \bar{u}_0 \bar{u}_{0\eta} + \bar{w}_0 \bar{u}_{0\eta} - \lambda \eta \bar{u}_{0F} = -(G2X), \tag{5.7a}$$

$$-b_1 \bar{w}_{2F} + B(\bar{u}_0 \bar{w}_{1F} + \bar{u}_1 \bar{w}_{0F}) + (\bar{v}_1 \bar{w}_{0Y} + \bar{v}_0 \bar{w}_{1Y}) + \lambda(\bar{w}_0 \bar{w}_{1F} + \bar{w}_1 \bar{w}_{0F}) - \mu \bar{u}_0 \bar{w}_{0\eta} + \bar{w}_0 \bar{w}_{0\eta} - \lambda \eta \bar{w}_{0F} = -(G2Z), \tag{5.7b}$$

with

$$G2X = \{(\mathrm{i} B g_{21} - \mu g_{11\eta} + \lambda \mathrm{i} \eta g_0) E + O(E^2)\} + \text{c.c.} - \mu g_{10\eta}, \tag{5.7c}$$

$$G2Z = \{(\mathrm{i}\lambda g_{21} + g_{11\eta}) E + O(E^2)\} + \text{c.c.} + g_{10\eta}. \tag{5.7d}$$

Concerning the mean-flow effects proportional to E^0 alone, we therefore obtain, from (5.5*a*) coupled with (5.7*a*, *b*), the *total mean-flow equations*

$$-\mu \overline{\bar{u}}_\eta + \bar{v}_{1Y} + \overline{\bar{w}}_\eta = 0, \tag{5.8a}$$

$$(-\mu \overline{\bar{u}} + \overline{\bar{w}}) \overline{\bar{u}}_\eta + \bar{v}_1 \overline{\bar{u}}_Y + \{(-\mu \bar{u}_{01} + \bar{w}_{01}) \bar{u}^*_{01\eta} + \bar{v}_{01} \bar{u}^*_{11Y} - \mathrm{i}\lambda(\bar{w}_{01} \bar{u}^*_{11} + \bar{w}_{11} \bar{u}^*_{01})\} + \text{c.c.} = 0, \tag{5.8b}$$

$$(-\mu \overline{\bar{u}} + \overline{\bar{w}}) \overline{\bar{w}}_\eta + \bar{v}_1 \overline{\bar{w}}_Y + \{(-\mu \bar{u}_{01} + \bar{w}_{01}) \bar{w}^*_{01\eta} + \bar{v}_{01} \bar{w}^*_{11Y} + \mathrm{i} B(\bar{u}_{01} \bar{w}^*_{11} + \bar{u}_{11} \bar{w}^*_{01})\} + \text{c.c.} = 0, \tag{5.8c}$$

with $\overline{\bar{v}}_1$ denoting the mean-flow component in $\bar{v}_1$, $\bar{u}_{01}$ the E component in $\bar{u}_0$, and so on. On use of the solutions in (5.4*a*–*c*), (5.6*a*, *b*), and with the definition of the skewed mean velocity,

$$\overline{\bar{q}} \equiv \overline{\bar{w}} - \mu \overline{\bar{u}}, \tag{5.9}$$

(5.8*a*–*c*) then reduce to the governing equations

$$\overline{\bar{q}}_\eta + \overline{\bar{v}}_{1Y} = 0, \tag{5.10a}$$

$$\overline{\bar{q}\bar{q}}_\eta + \overline{\bar{v}}_1 \overline{\bar{q}}_Y = \mathscr{G}(\eta), \tag{5.10b}$$

for $\overline{\bar{q}}, \overline{\bar{v}}_1$. Here $-\mathscr{G}(\eta)$ is the effective pressure gradient, given by

$$-\mathscr{G} = (\mu^2 + 1)(B^2 + \lambda^2) b_1^{-2} (|g_0|^2)_\eta, \tag{5.10c}$$

and the main boundary conditions are

$$\overline{\bar{q}} \sim -\mu Y + o(Y^{-1}), \quad \overline{\bar{v}}_1 \sim -\mu^{-1} \mathscr{G} + O(Y^{-1}), \quad \text{as} \quad Y \to \infty, \tag{5.11a}$$

$$\overline{\bar{v}}_1 = 0 \quad \text{at} \quad Y = 0, \tag{5.11b}$$

in view of the matching in (5.4d, e), along with (5.9) and (5.10a, b), and the surface tangential-flow requirement respectively.

The total mean flow in this wall layer is controlled essentially, then, by the 2D inviscid boundary-layer equations (5.10a, b) subject to (5.11a, b). The major point now is that the mean-flow quantities appear to be *arbitrary* here, since differentiation of (5.10b) with respect to Y shows that the mean skewed shear or vorticity, $\overline{\overline{\tau}} \equiv \partial\overline{\overline{q}}/\partial Y$, is an arbitrary function of the mean skewed streamfunction $\overline{\overline{\psi}}$,

$$\overline{\overline{\tau}} = \overline{\overline{\tau}}(\overline{\overline{\psi}}), \tag{5.12}$$

where $\overline{\overline{q}} = \partial\overline{\overline{\psi}}/\partial Y$, with $\overline{\overline{\psi}} = 0$ at $Y = 0$ say, and the only significant restriction on $\overline{\overline{\tau}}GM$ is that $\overline{\overline{\tau}} \sim -\mu + o(Y^{-2})$ at large Y. This arbitrariness in the solution for $\overline{\overline{q}}, \overline{\overline{v}}_1$, and hence in $\overline{\overline{u}}, \overline{\overline{w}}$, reflects the dependence of the present nonlinear large-time behaviour on the initial state at zero time, and subsequently, we believe, and it affects the entire nonlinear response significantly, as shown later. It is also a little reminiscent of the arbitrariness in the vorticity for the purely 2D initial-value problem, referred to in §1, although in contrast with that case the vorticity here cannot be simple, as the solution for $\overline{\overline{q}}$ does not admit a trivial form. Certain helpful features can be written down explicitly, nevertheless. Thus the constraint (5.11b) inserted in (5.10b) yields on integration the Bernoulli relation

$$\overline{\overline{q}}^2|_{Y=0} = -2(\mu^2+1)\,(B^2+\lambda^2)\,b_1^{-2}|g_0|^2 + \text{const.}, \tag{5.13}$$

which, because of the signs involved, indicates that the mean-flow effect must persist outside the current zone of $O(1)$ values of η. Similar relations hold for the individual components $\overline{\overline{u}}, \overline{\overline{w}}$. Again, the mean efflux velocity $\overline{\overline{v}}_1$ in (5.11a) is consistent with the value of v_{20}, in §3, at small s, and other matching conditions can also be verified.

The arbitrariness in the mean flow persists at higher order also. In particular, the mean-flow-correction velocity $\overline{\overline{u}}_1$ in (5.6a) remains arbitrary, apart from the matching condition

$$\overline{\overline{u}}_1 \sim \chi_L \ln Y + \overline{\overline{A}}_1, \quad \text{as} \quad Y \to \infty, \tag{5.14}$$

with $\overline{\overline{A}}_1$ being an arbitrary function of η. Here (5.14), coupled with the requirement that the mean-flow term $\overline{\overline{u}}_{1L}(\eta, Y)$ remains finite at large Y, merges the wall-layer behaviour with that in (3.12a) ff. involving u_{10}, u_{10L}; similarly, the tangential-flow constraint imposed near the end of §3, concerning A_{10L}, is necessary for the merging with the response in the present wall layer, since a non-zero $O(\hat{X}\ln\hat{X})$ E-contribution in $\hat{V}$ would be inconsistent with the condition of tangential flow at $Y = 0$. The unknown wall-layer displacement term $\overline{\overline{A}}_1$, however, has a profound effect, since it is equal to the mean-flow bulk-displacement term A_{10} in (3.11a), to within an additive constant. Hence $A_{10}(\eta)$ is also arbitrary, in the sense above, and that arbitrariness then feeds into v_{20} and the nonlinear critical-layer solution of §4 as well (see q_4), and more significantly into the amplitude equation for g_0 in §6 below. It might be argued further than an arbitrary displacement effect, $\overline{\overline{A}}(\eta)$ say, could be present in the total mean-flow solution in the wall layer, corresponding to adding $\overline{\overline{A}}$ to Y in (5.11a) and in (5.4d, e). This would induce an $O(\hat{X}^{\frac{1}{3}})$ mean-flow correction of U in the bulk flow of §3, however, comparable with the fundamental, and (as such) would appear to alter the ordering, starting in §3, to a very significant extent. Although that cannot be ruled out (after all, we do not claim uniqueness), it is felt to be tantamount to the introduction of a completely new type of nonlinear disturbance; see also the comments on large-amplitude effects in the following sections.

PHILOSOPHICAL TRANSACTIONS OF THE ROYAL SOCIETY A MATHEMATICAL, PHYSICAL & ENGINEERING SCIENCES

6. The external relations, and the amplitude equations

The analysis in §§3–5 yields general 'internal' relations in effect, between the pressure and displacement components, that apply to any flow governed by the large-time boundary-layer-like equations of (2.6*a–e*). It remains to impose the 'external' relations of (2.7) or (2.8*a–c*) which are specific to the present context of the incompressible 3D boundary layer. Below we continue first with the case $\kappa = 1$, in §6*a*, before modifying the analysis to the case $\kappa = \hat{X}^{-\frac{1}{3}}$ in §6*b*.

(*a*) *The* $\kappa = 1$ *case*

The external pressure expansion, in line with the internal one (3.1*d*), is of the form

$$\bar{p} = \hat{X}^{\frac{4}{3}}(E\bar{g}_0 + \text{c.c.}) + \ldots + \hat{X}^{\frac{2}{3}}(E\bar{g}_{12} + \ldots) + \ldots + (E^3\bar{g}_{23} + \ldots) + \ldots, \tag{6.1}$$

but with the components $\bar{g}_0$, etc., being dependent on the normal coordinate $\bar{\bar{y}}$, of order unity now, where the fast scaling $\bar{y} = \hat{X}^{-1}(1+\mu^2)^{-\frac{1}{2}}\bar{\bar{y}}$ is implied by the fast $\hat{X}$-dependence present in E, etc. So here

$$\partial_{\hat{X}} \to \partial_{\hat{X}} - \left(\mu\hat{X}^{\frac{1}{3}} - \frac{\eta}{3\hat{X}}\right)\partial_\eta + \frac{\bar{\bar{y}}}{\hat{X}}\partial_{\bar{\bar{y}}}, \quad \partial_{\hat{Z}} \to \hat{X}^{\frac{1}{3}}\partial_\eta, \quad \partial_{\bar{y}} \to (1+\mu^2)^{\frac{1}{2}}\hat{X}\,\partial_{\bar{\bar{y}}}. \tag{6.2}$$

Substitution into (2.8*a*) therefore leads to the successive governing equations

$$\mathscr{D}(\bar{g}_0) = 0, \quad \mathscr{D}(\bar{g}_{11}) = 2\mathrm{i}(\mu B - \lambda)\,\bar{g}_{0\eta}, \tag{6.3a, b}$$

$$(\mathscr{D} - 3(B^2+\lambda^2))\,(\bar{g}_{12}) = 0, \quad \partial^2_{\bar{\bar{y}}}(\bar{g}_{10}) = 0, \tag{6.3c, d}$$

$$\mathscr{D}(\bar{g}_{21}) = 2\mathrm{i}(\mu B - \lambda)\,\bar{g}_{11\eta} - (\mu^2+1)\,\bar{g}_{0\eta\eta} + 2\lambda B\eta\bar{g}_0, \tag{6.3e}$$

where the operator $\mathscr{D}$ is defined by

$$\mathscr{D} \equiv (1+\mu^2)\,\partial^2_{\bar{\bar{y}}} - (B^2+\lambda^2), \tag{6.4}$$

and (6.3*b–e*) show the gradual intrusion of the slowly varying dependence present. The boundary conditions require boundedness at large $\bar{\bar{y}}$, essentially, and, as $\bar{\bar{y}} \to 0+$, the pressure matching $\bar{g}_n \to g_n$ ($n = 0, 11$, etc.) and the normal velocity matching $(1+\mu^2)^{\frac{1}{2}}\partial_{\bar{\bar{y}}}\bar{g}_0 \to -B^2A_0$, etc., from (2.8*b*, *c*).

Hence at leading order we have the solution, from (6.3*a*),

$$\bar{g}_0 = g_0 \exp(-\gamma\bar{\bar{y}}), \quad \text{with} \quad \gamma \equiv (B^2+\lambda^2)^{\frac{1}{2}}(1+\mu^2)^{-\frac{1}{2}}, \tag{6.5}$$

which yields the first external pressure–displacement relation

$$(1+\mu^2)^{\frac{1}{2}}\gamma g_0 = B^2A_0. \tag{6.6}$$

Similar working applies to the higher-order components in (6.3*b–e*), giving the results

$$(1+\mu^2)^{\frac{1}{2}}(\gamma g_{11} - \pi_{11}) = B^2A_{11} + 2\mu\mathrm{i}BA_{0\eta}, \tag{6.7}$$

$$(1+\mu^2)^{\frac{1}{2}}\gamma g_{12} = 2B^2A_{12}, \tag{6.8}$$

$$\bar{g}_{10} = g_{10} \equiv 0, \tag{6.9}$$

$$(1+\mu^2)^{\frac{1}{2}}(\gamma g_{21} - \pi_{21}) = B^2A_{21} + 2\mu\mathrm{i}BA_{11\eta} + 2\lambda B\eta A_0 - \mu^2A_{0\eta\eta} \tag{6.10}$$

for the higher-order external relations. Here

$$\pi_{11} = \mathrm{i}(\lambda - B\mu)\,\gamma^{-1}(1+\mu^2)^{-1}\,g_{0\eta},$$

$$\pi_{21} = \{2\mathrm{i}(\lambda - B\mu)\,g_{11\eta} + (\mu^2+1)\,g_{0\eta\eta} - 2\lambda B\eta g_0 + \mathrm{i}\gamma^{-1}(\lambda - B\mu)\,\pi_{11\eta}\}/\{2\gamma(1+\mu^2)\}.$$

Further, the result (6.9) for the mean-pressure correction is that anticipated in §3 and is due to the lack of fast dependence in the mean-flow contributions; indeed, the mean-flow displacement E^0A_{10} forces a non-zero pressure feedback only at higher order, namely

$$g_{20} = (1+\mu^2)^{-\frac{1}{2}}\frac{\mu^2}{\pi}\int_{-\infty}^{\infty}\frac{A_{10\xi}\,\mathrm{d}\xi}{(\eta-\xi)}, \tag{6.11}$$

via the quasi-planar properties holding on a larger external normal scale of $\bar{y} \sim \hat{X}^{-\frac{1}{3}}$. We proceed now to couple (6.6)–(6.10) with the internal relations of §3.

First, (3.6d) with (6.6) gives the balance

$$b_1 = B(B^2+\lambda^2)^{\frac{1}{2}}, \tag{6.12}$$

which is effectively the dominant eigenrelation, leaving g_0 arbitrary. Second, (3.8d) with (6.7) likewise leaves g_0, g_{11} arbitrary so far, but imposes the second eigenrelation

$$\lambda b_1 = \mu(B^2+\lambda^2). \tag{6.13}$$

Here, given the value of μ, i.e. the direction of the edge region (see §2), the results (6.12), (6.13) (and the definition in (3.2a)) serve to fix the other constants b_1, B, λ. For the specific case of the angle $\arcsin\frac{1}{3} = 19.47°$, corresponding to linear behaviour holding everywhere *outside* the edge region, the constants are

$$\mu = 8^{-\frac{1}{2}}, \quad b_1 = 3^{\frac{3}{2}}/16, \quad B = 3^{\frac{1}{2}}/4, \quad \lambda = (3/8)^{\frac{1}{2}}, \tag{6.14}$$

consistent with the previous linear theory (Doorly & Smith 1992). Third, (3.7d) and (6.8) determine the second-harmonic amplitudes in terms of the unknown fundamentals,

$$g_{12} = -B^{-2}g_0^2, \quad A_{12} = -\tfrac{1}{2}b_1B^{-5}g_0^2. \tag{6.15a, b}$$

The results above allow some simplifications in the expressions for the coefficients present in the solutions of §3, and details of these simplifications are available from the author. Fourth, the implied mean-flow-correction effects at this stage are covered by the results (3.9) ff., (6.9), (6.11), the primary feature overall being that A_{10} remains arbitrary; see also §5. Fifth, the combination of (6.10) and the solutions in (3.13a, b), along with the critical-layer and wall-layer responses of §§4 and 5, leads to the amplitude equation for $g_0(\eta)$, as follows.

In essence, the internal pressure–displacement relation between g_{21}, A_{21} follows from setting $s \to 0+$ in (3.3e), (3.13b) and imposing the match with the wall-layer solution of §5, a match which involves singular contributions of order s^{-1} and $\ln s$ as well as the $O(1)$ terms. This process leaves the internal relation as, for $s \to 0+$,

$$b_1\left[\int_s^{\infty}\delta^{-1}B_{21}\,\mathrm{d}s - \mathrm{i}A_{21}\right] + v_{21} \sim -\mathrm{i}Bg_{21} + \mu g_{11\eta} - \mathrm{i}\lambda\eta g_0 + \lambda\mathrm{i}\eta u_0 - \mathscr{M}_{21}, \tag{6.16}$$

formally, where the small s behaviour present follows from (3.12a, b), (3.15a–c). Here, after some working, the $O(s^{-1})$ and $O(\ln s)$ terms are found to cancel out, as expected. Then the coupling with the external relation (6.10) leads to cancellation of all the $g_{21}, g_{11}, g_{11\eta}$ terms also, on use of the previous results in this section, leaving as a solvability condition the amplitude equation

$$\mathscr{T}_1 g_{0\eta\eta} - \mathscr{T}_2\,\eta g_0 = -b_1 I - \mathscr{M}_{21}(\mathrm{F.P.}), \tag{6.17}$$

for $g_0(\eta)$, again after some working. Here F.P. denotes the finite part and

$$\mathscr{T}_1 = -\frac{4\mathrm{i}}{B}(B^2+\lambda^2)+\frac{\mathrm{i}(\mu^2+1)}{2B}+\frac{5\mathrm{i}\mu^2}{B^3}(B^2+\lambda^2)-\frac{\mathrm{i}(\mu B-\lambda)^2\mu^2}{2\lambda^2B^3}-2\mathrm{i}(\mu B-\lambda)\frac{\mu}{B^2}, \quad (6.18a)$$

$$\mathscr{T}_2 = \mathrm{i}\lambda b_1^{-1}B^{-2}[-\lambda^3\mu+b_1(\mu^2+\lambda^2)], \quad (6.18b)$$

$$I = -\frac{\mathrm{i}\lambda^2|g_0|^2g_0}{2b_1B^5}+(\mathrm{F.P.})\int_0^\infty \delta^{-1}\overline{\overline{Q}}\,\mathrm{d}s; \quad (6.18c)$$

further details here and below are available from the author. In the specific case of (6.14), therefore,

$$\mathscr{T}_1 = 3^{\frac{1}{3}}\mathrm{i}/2, \quad \mathscr{T}_2 = \mathrm{i}(2/3)^{\frac{1}{2}}, \quad (6.19a, b)$$

and these values provide a check on the analysis. For the right-hand side of (6.17) contains all the nonlinear amplitude-cubed effects and so, for a *linear* disturbance, (6.17) reduces to Airy's equation for $g_0(\eta)$, giving the solution

$$g_0 \propto \mathrm{Ai}\,(3^{-\frac{1}{3}}2^{\frac{1}{3}}\eta) \quad (6.20)$$

in terms of the Airy function Ai, for the case of (6.14), (6.19*a*, *b*). The solution (6.20) agrees with the previous linear theory, as required.

In the *nonlinear* régime, however, the full amplitude equation (6.17) applies. The most interesting feature then is that the nonlinear coefficient (of $|g_0|^2g_0$ below) is influenced by the mean-displacement term A_{10}, through $\overline{\overline{Q}}, \mathscr{M}_{21}$ in (6.17), (6.18*c*), (3.11*a*), (3.14*d*, *f*) and, since §5 shows A_{10} to be arbitrary (although real), the nonlinear coefficient is also arbitrary. (Again see the comment immediately after (6.18*c*) above.) So (6.17) becomes, in a normalized form,

$$g_{0\hat{\eta}\hat{\eta}}-\hat{\eta}g_0 = \hat{a}|g_0|^2g_0, \quad (6.21)$$

where $\hat{\eta} \equiv (\mathscr{T}_2/\mathscr{T}_1)^{\frac{1}{3}}\eta$ and the coefficient $\hat{a}$ is real but arbitrary, in the sense of being dependent upon the development of (2.6) ff. at $O(1)$ scaled distances before the large-distance form of (2.9) ff., it is felt. Here the form of the nonlinearity follows from A_{10} being real and proportional to $|g_0|^2$, in keeping with the order at which this nonlinear effect arises. As far as we can tell, a non-zero imaginary part for $\hat{a}$ or another type of nonlinearity cannot be produced for example by the critical layer in the present setting.

A further normalization, $g_0 = 2^{\frac{1}{3}}|\hat{a}|^{-\frac{1}{3}}g$, reduces the governing equation to the second Painlevé transcendent, namely

$$g''-\hat{\eta}g\pm 2g^3 = 0 \quad (6.22)$$

(the prime denotes $\mathrm{d}/\mathrm{d}\hat{\eta}$), for $\hat{a}$ negative or positive respectively, subject to the condition

$$g \sim \frac{\tilde{a}}{2\pi^{\frac{1}{3}}\hat{\eta}^{\frac{1}{4}}}\exp(-\tfrac{2}{3}\hat{\eta}^{\frac{3}{2}}) \quad \text{as} \quad \hat{\eta}\to\infty. \quad (6.23)$$

Here g_0, g are assumed real without loss of generality, the condition (6.23) corresponds to linear properties holding outside the edge region and is in line with (6.20), while the parameter $\tilde{a}$, representing a combined measure of the disturbance amplitude and the mean displacement effect, is arbitrary in the sense defined previously. The form (6.22$\pm$), (6.23) is exactly that studied by Miles (1978) and Rosales (1978), and our interest, like theirs, is in the behaviour of the solution $g(\hat{\eta})$ for any prescribed $\tilde{a}$ value.

PHILOSOPHICAL TRANSACTIONS OF THE ROYAL SOCIETY A MATHEMATICAL, PHYSICAL & ENGINEERING SCIENCES

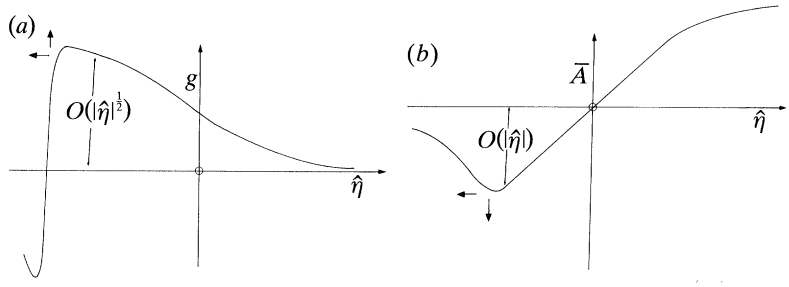

Figure 2. The influence of increasing input amplitude on the wing-tip solution behaviour, (*a*) for case I (see §6*a*), (*b*) for case II (see §6*b*). The solid arrows indicate the directional effects due to increased nonlinearity.

A minor point, however, is that unlike these last authors we would not necessarily restrict g to be bounded: see below. As $\tilde{a}$ is increased the solution of (6.22), (6.23) deviates increasingly from the Airy form equivalent to that in (6.20) as Rosales' (1978) results show. Of most concern next is the solution response at extreme $\tilde{a}$ values (figure 2). There appear to be three main alternatives, at least two of which are as described in Miles' (1978) detailed analysis. The first is essentially that

$$|g| \propto |\hat{\eta}|^{\frac{1}{2}} \quad \text{at large} \quad |\hat{\eta}|, \tag{6.24}$$

before attaining the asymptote (6.23); see also Hastings & McLeod (1982). In the second, a finite-distance singularity occurs in which

$$g \propto |\hat{\eta} - \hat{\eta}_0|^{-1} \quad \text{as} \quad \hat{\eta} \to \hat{\eta}_0 \pm, \tag{6.25}$$

with $\hat{\eta}_0$ a finite constant. The third alternative has, in order-of-magnitude terms,

$$g \propto \tilde{\delta}^{-\frac{1}{3}} \quad \text{where} \quad \hat{\eta} - \hat{\eta}_1 \sim \tilde{\delta}^{\frac{2}{3}}, \quad \tilde{\delta} = |\hat{\eta}_1|^{-\frac{3}{2}} \tag{6.26}$$

and $|\hat{\eta}_1|$ is large. Miles shows that (6.24), (6.26) agree satisfactorily with the computational results of Rosales. The three alternatives above correspond to $\tilde{a}$ being near 1, typically $O(1)$, and large, respectively, with (6.24), (6.26) applying to (6.22$\mp$) in turn. The properties (6.24)–(6.26) also have broad implications for the influence of increased nonlinearity in the far-downstream large-time behaviour which are considered in §7. Before that, however, we must turn to the alternative case anticipated at the end of §2 and the start of §3.

(*b*) *The* $\kappa = \hat{X}^{-\frac{1}{3}}$ *case*

The existence of this alternative hinges on the issue of whether there is a significant nonlinear wall layer or not, and especially on the behaviour in (3.12*a*) ff. For if, instead of the response in §3 leading to the wall layer of §5, the equivalent of a tangential-flow condition is imposed on the bulk mean flow in §3, then the mean pressure term g_{10} must be non-zero. In consequence, the mean displacement is increased by an order $\hat{X}^{\frac{2}{3}}$ in relative terms, in view of the external relations as in §6.1 and the slow variation of the mean-flow quantities, leading to an analogue of (6.11). This increase, which accentuates the influence of the mean-flow correction on the nonlinear solution behaviour, is the basis for the re-ordering associated with

$$\kappa = \hat{X}^{-\frac{1}{3}}. \tag{6.27}$$

With (6.27) holding, along with the bulk-flow expansion in (3.1*a*–*e*), much of the working in §§3–5 and §6*a* stays intact. It is as if terms $E^{\pm N}$ for the $\kappa = 1$ case are

replaced by $\kappa^N E^{\pm N}$ now except for the mean g_{10} term in (3.1d); the extra factors κ^N act to suppress certain nonlinear contributions in favour of others, while leaving unaltered the coefficients in the equations for the favoured terms since the fast dependence $E^{\pm N}$ dominates the derivatives involved, with a small relative error of order $\hat{X}^{-2}$. Thus the second-harmonic contributions for instance tend to become suppressed. Further details are presented in Appendix B, the main points being that a weaker motion close to the wall demands that

$$g_{10} = -(B^2+\lambda^2)\, b_1^{-2}\, g_0\, g_0^*, \tag{6.28a}$$

while the external flow yields the relation

$$g_{10} = \frac{\mu^2(1+\mu^2)^{-\frac{1}{2}}}{\pi} \int_{-\infty}^{\infty} \frac{A_{10\xi}\, \mathrm{d}\xi}{(\eta-\xi)} \tag{6.28b}$$

for the displacement, and then the nonlinear effect on the main amplitude equation, obtained as a solvability requirement, is dominated by the new mean-flow displacement, giving

$$\mathscr{T}_1\, g_{0\eta\eta} - \mathscr{T}_2\, \eta g_0 = -\mathrm{i}(B^2+\lambda^2)\, b_1^{-1}\, A_{10}\, g_0. \tag{6.28c}$$

Here (6.28a–c) follow from the modifications of (3.12a) ff., (6.11), (6.16) ff. respectively, due to the new ordering (6.27). Combining (6.28a–c), and setting

$$[g_0, A_{10}, \eta] = \left[\frac{\mu b_1^{\frac{3}{2}} (\mathscr{T}_2/\mathrm{i})^{\frac{1}{2}}}{(B^2+\lambda^2)\,(1+\mu^2)^{\frac{1}{4}}} g,\ \frac{b_1}{(B^2+\lambda^2)} \left(\frac{\mathscr{T}_2}{\mathrm{i}}\right) \left(\frac{\mathscr{T}_1}{\mathscr{T}_2}\right)^{\frac{1}{3}} \bar{A},\ \left(\frac{\mathscr{T}_1}{\mathscr{T}_2}\right)^{\frac{1}{3}} \hat{\eta}\right], \tag{6.29}$$

we therefore obtain the normalized amplitude equation(s)

$$g'' - \hat{\eta} g = -\bar{A} g, \quad \text{where} \quad -g^2 = \frac{1}{\pi} \int_{-\infty}^{\infty} \frac{\bar{A}_s\, \mathrm{d}s}{(\hat{\eta}-s)}, \tag{6.30a, b}$$

governing $g(\hat{\eta})$ (and $\bar{A}(\hat{\eta})$). The system (6.30a, b), together with zero conditions on $g(\pm\infty)$ (e.g. as in (6.23)), replaces (6.22) or its earlier forms (6.17), (6.21). At low amplitudes the equivalent of the Airy solution (6.20) applies of course, whereas at most amplitudes (6.30a, b) require a computational treatment.

Computational results for (6.30a, b) were obtained by a finite-difference method described in Appendix C and are summarized in figure 3. The Airy form is confirmed at low amplitudes, but as the amplitude is increased to $O(1)$ or larger the characteristic $\hat{\eta}$-scale appears to increase. This leads to the account of the multi-structured solution behaviour at *high* amplitudes, presented in Appendix D and figure 4. There the $\hat{\eta}$ scale and the $\bar{A}$ scale both increase indefinitely but $|g|$ remains $O(1)$, typically, with

$$|\bar{A}| \sim |\hat{\eta}| \text{ large}, \quad |g| = O(1), \tag{6.31}$$

apart from thin regions where the variation in $|\bar{A}|$ is lessened, $|\hat{\eta}|$ is small (with an origin shift), and $|g|$ can be large; see also figure 2. The response in (6.31) ff. and Appendix D, for increasing amplitudes, points to the effects of stronger nonlinearity discussed in the next section.

7. Further discussion

The aim in this work is to obtain some guidance on 3D amplitude-dependent effects in spot development in an incompressible boundary layer and start to build up a picture of the flow structure in a typical nonlinear spot. Such a picture seems

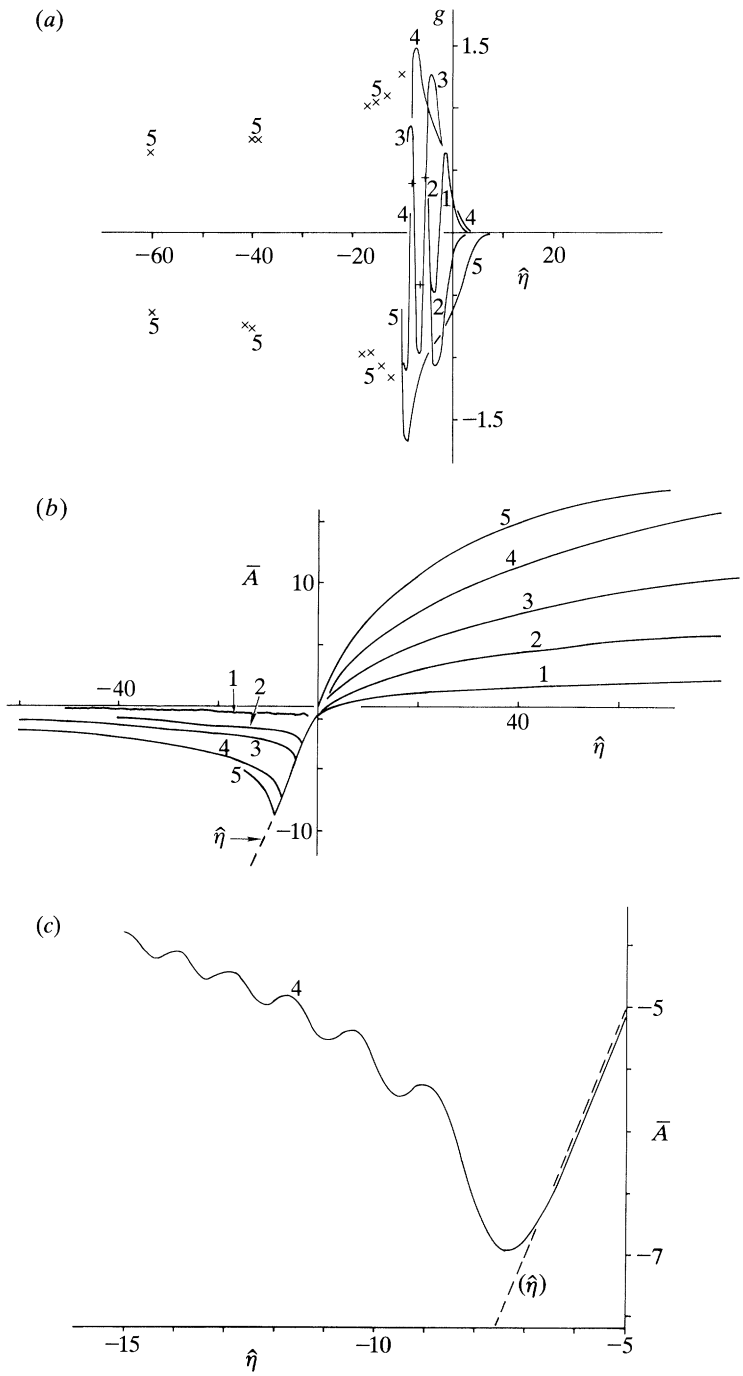

Figure 3. Computational solutions (marked 1–5) of (6.30*a*, *b*) for case II: (*a*) g, (*b*) $\bar{A}$, versus $\hat{\eta}$, at various amplitudes. In (*a*), the results ×, + are sample extrema for the solutions marked 5, 1 in turn. See also Appendix C. In (*b*), the line $\bar{A} = \hat{\eta}$ is added for comparison purposes; see figure 4, and Appendix D. A magnified view of (*b*) is given in (*c*) and shows significant oscillations present in $\bar{A}$, which are in line with the theory in Appendix D.

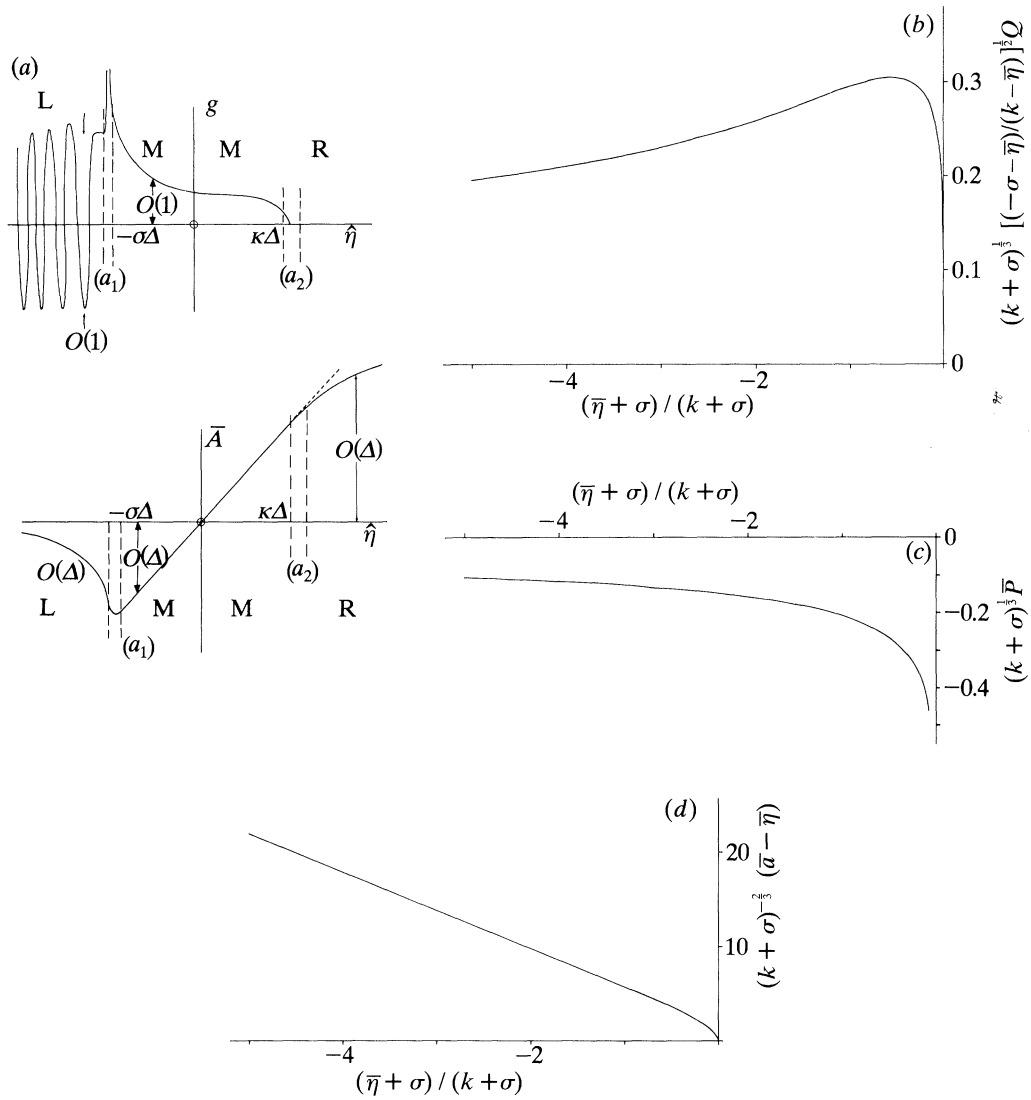

Figure 4. (*a*) The structure (for case II) of the solution of (6.30*a*, *b*) at large amplitudes, showing the three main regions *L*, *M*, *R* (see §6.2, Appendix D) and the thinner adjustment zones a_1, a_2. Here Δ is large. (*b*)–(*d*) A computational solution for the large-amplitude behaviour in region L (case II), from (D 16) ff. in Appendix D, showing (*b*) the integrand of (D 16), (*c*) the effective pressure, (*d*) the displacement effect.

to be emerging a little now, as described below, from the present study of nonlinear edge-layer dynamics near the wing tips.

In §§3–6 above, linear properties continue to hold outside the edge layer(s), leading in particular to the prediction of 19.47° for the wake half-angle (Doorly & Smith 1992) unless there is some extra forcing present for example. Inside the edge layer, on the other hand, several interesting features arise as nonlinearity first enters play in the large-time large-distance analysis. Let us address case I first, where

$$\kappa = 1. \tag{7.1}$$

PHILOSOPHICAL TRANSACTIONS OF THE ROYAL SOCIETY A MATHEMATICAL, PHYSICAL & ENGINEERING SCIENCES

This leads to nonlinear wall and critical layers being generated (§§4 and 5), with the latter exhibiting a checkerboard pattern of closed streamlines. The mean vorticity produced appears at present to contain a degree of indeterminacy for large times and distances, along with the displacement effects, to the level of the working here at least, due possibly to the vortex stretching present in 3D although there is bound to be some degree of arbitrariness anyway, associated with the initial conditions. We note that in fact some mean-flow displacements are taken to be zero right at the outset of §3, and the corresponding mean-flow correction has maximum relative effect in the wall layer and the critical layer. In turn, the additional nonlinear contribution to the Airy equation describing the edge-layer response contains an arbitrary coefficient: see §6*a*. More significantly, however, as the characteristic amplitudes present in the edge layer increase the influence of nonlinearity can spread from the edge layer towards increasingly negative or positive values of η, i.e. heading for the middle portion of the spot in the former case (see figure 2 again). The implications of this can be seen from the extreme properties (6.24)–(6.26). Thus (6.24) leads to a typical pressure $\hat{p}$ of magnitude *ca.* $\hat{X}^{\frac{4}{3}}|\hat{\eta}|^{\frac{1}{2}}$ (using (3.1*d*)) as $|\hat{\eta}|$ increases, i.e. as $(\hat{Z}-\mu\hat{X})\hat{X}^{\frac{1}{3}}$ increases. Hence when the middle portion of the spot is entered, where $\hat{Z}/\hat{X}-\mu$ is $O(1)$ typically, $|\hat{\eta}|$ becomes $O(\hat{X}^{\frac{4}{3}})$ and so $\hat{p}$ increases to the magnitude $O(\hat{X}^2)$. Likewise, (6.26) yields the same magnitude, as $|\hat{\eta}_1|\to O(\hat{X}^{\frac{4}{3}})$, along with a faster local spatial scale of order X^{-1}, which is also implied by (6.25). The dominant new impact here then is twofold: strong nonlinearity tends to spread right across the spot, as well as developing shorter length scales within the spot, in contrast both with linear disturbances and with the nonlinear ones of §§3–6. The new behaviour proposed above points to a subsequent study (Smith 1992) of the middle portion of the spot, based on the predictions just mentioned and with significant differences to be expected compared with the previous linear régime.

For the alternative case II, in which

$$\kappa = \hat{X}^{-\frac{1}{3}}, \tag{7.2}$$

some of the above points still apply but the overall implications are rather different; see §6*b*. For a start, the wall layer is much less significant, and the main nonlinear influence is due to the induced mean-flow displacement. In addition, the influence of increased nonlinearity in the edge layer seems to produce a definitive *inward* trend towards the middle of the spot, subject to an origin shift in $\hat{\eta}$ absorbing a constant term in $\bar{A}$ in §6*b*. (The inward trend here stems from the result (6.28*a*) that the mean pressure produced is negative, see also (6.30*b*) and Appendix D.) Thus the characteristic pressure $\hat{p}$ now has magnitude *ca.* $\hat{X}$ and the displacement $-\hat{A}$ is $O(1)$ mainly, but the mean displacement increases like $\hat{X}^{-\frac{1}{3}}|\hat{\eta}|$, from (3.1*d*, *e*), (6.31) with (7.2), at increased amplitudes. So the suggestion is that nonlinearity again floods into the middle portion of the spot, where $|\hat{\eta}|$ becomes $O(\hat{X}^{\frac{4}{3}})$ in essence and forces the mean displacement to rise to the order $\hat{X}$. The latter represents a strongly nonlinear effect, since the typical mean velocity is also $O(\hat{X})$ (see (3.1*a*)); yet the oscillatory part of the displacement stays relatively small, in contrast with the previous paragraph. Smaller length scales also develop, in line with the comments just after (6.31) above.

Clearly, the flow features provoked by stronger nonlinearity as described in the previous two paragraphs, and in figure 5, are of much concern, and resulting studies are in progress. A main zone for such more nonlinear spots would seem to be further downstream, at streamwise distances proportional to time (Doorly & Smith 1992) but with a typical fast spatial scale acting of order unity, rather than at distances of

PHILOSOPHICAL TRANSACTIONS OF THE ROYAL SOCIETY A MATHEMATICAL, PHYSICAL & ENGINEERING SCIENCES

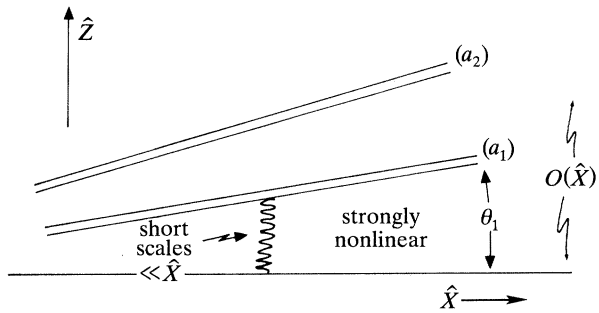

Figure 5. Schematic diagram of the next stage, encountered at higher input amplitudes, according to §7. Case I leads to only one typical adjustment zone a_1, whereas case II yields two, a_1, a_2, which are continuations of those in figure 4(*a*). The amplitudes and short length scales involved are also different, as explained in §7, but in both cases the middle of the spot is now strongly nonlinear and the spreading angle θ_1 is now different from the angle θ_0 of figure 1.

order (time)$^{\frac{1}{2}}$ as in §§2–6 above. In the main zone nonlinear travelling waves or solitary waves seem likely, certainly if $\kappa = 1$, and possibly even finite-time singularities (Stuart & Tabor 1990). The solution can be matched back to the current (time)$^{\frac{1}{2}}$ zone, however, to yield the 19.47° prediction for example if the amplitudes involved are not too large, as a relatively small-distance asymptote. This picture is broadly consistent with the simpler 2D case in the context of thin-layer flow, where the Benjamin–Ono equation applies and yields a main nonlinear O(time) zone supplemented by the O(time)$^{\frac{1}{2}}$ scale. The current extension to the more complex 3D case for full Euler flow is of more interest, of course, including the perhaps surprising feature that the O(time)$^{\frac{1}{2}}$ zone for Euler flow is governed by a triple-deck interaction (§2).

Aside from the present research on nonlinearity and its immediate consequences, there are a number of other physical processes that are significant in real spot evolution and are far from fully understood. Viscous effects are certainly very significant (Walker 1990, etc.) and they can enter the reckoning in several ways, e.g. at large times in the third context described in §2 or at $O(1)$ times through break-up singularities and sublayer bursting (Smith 1988; Peridier *et al.* 1991; Hoyle *et al.* 1991); cf. also the $O(Re^{-\frac{1}{4}})$ scale in Smith & Burggraf (1985). The domino process mentioned in §1 could well be connected with successive occurrences of the finite-time break-up in Smith (1988), as in a chain reaction. Again, no uniqueness is claimed in the theoretical work as we are seeking particular forms of nonlinear effects. There may well be some flows in which the mean-flow displacement is stronger than that in §§3–6; see also earlier comments, e.g. in §5. Indeed, we favour the description given by case II (in §6*b*), in which the 3D mean-flow displacement yields the dominant nonlinear effect, rather as in vortex-wave interactions. For, in case II, the wall layer is relatively weak, as (6.28*a*) cancels out the driving pressure gradient (5.10*c*) effectively, in contrast with case I where the wall-layer motion is strong and even has to persist substantially beyond the edge-layer region, which seems an unlikely occurrence. Other forms may feel the impact of other vortex-wave interactions (Hall & Smith 1991), of possible wave resonances, of pressure–displacement viscous–inviscid interaction (see previous references in this paragraph), of nonlinear unsteady critical layers, of 3D vortex applications stemming from §2 (as in Smith 1987), and so on; see also other references in §1.

Regarding connections with experiments, it is almost certainly too early to expect

direct quantitative comparisons to be feasible. Nevertheless, as far as the present theoretical findings are concerned directly, possible agreement of a qualitative nature can be claimed with Glezer *et al.*s (1989) and others' experimental emphasis on substantial wing-tip and trailing effects. In broad terms, moreover, the overall picture emerging above, of a nonlinear multi-wave form flooding the middle and main zones of the spot, at increased amplitudes, and supplemented by successive viscous-sublayer eruptions (see 'domino process' above) and induced smaller scales, appears to be possibly in line with most spot experiments (D. J. Doorly, personal communications); see also references in §1. Also the longitudinal vortex formations suggested by §6*b* seem to be observed in some of the recent experiments; and it is intriguing that the description in §6*b* may lead to a logarithmic profile for the higher-order mean streamwise velocity correction near the wall. On the other hand, the theory so far rather over-estimates the spread angle of the spot in comparison with observations, and, as Sir James Lighthill has pointed out (personal communications), the relatively abrupt natures of both the wing-tips and the leading edge observed in a turbulent spot have still to be explained fully. Against that, however, the spread angle is altered by nonlinearity as described in figure 5 and above (cf. the alterations due to viscosity and compressibility (Doorly & Smith 1992)), and it is felt that the beginnings of an explanation for the abrupt wing-tips may well be provided by the results (6.24), (6.31) (and see figures 2–5), at increased amplitudes. Satisfactory theoretical accounts for several other basic aspects of spots could well stem from the further nonlinear analysis and related computations to be performed, as indicated earlier in this section.

Meanwhile, more experiments and/or full computations on the effects of carefully controlled and gradually increased initial amplitudes on the downstream development of nonlinear spots could be extremely useful, partly to compare with the theoretical suggestions (mainly those of §6*b*) and partly for more clarification (see also Gaster 1990). Many extra issues of the present theory itself also remain to be investigated, including the influences of viscosity (cf. §3), the O(time) zones, and the mid-spot behaviour while (3.1) holds, and there are applications to compressible boundary layers (cf. Doorly & Smith 1992), jets, channel flows, wakes, free-surface flows and so on.

Thanks are due to Sir James Lighthill primarily, who provided the author with much encouragement on both the Euler stage in general and the current approach regarding nonlinear effects in spot development, to Dr R. I. Bowles, Dr D. J. Doorly and Dr M. Blair for their interest and comments, to the referees for their comments, and to Professor M. V. Berry and Professor D. H. Peregrine for pointing out certain references. Further research is to be reported in a review article by the author in the Journal of Engineering Mathematics in 1993/4, indicating among other things an interaction in which the wave and the mean-flow correction are reduced by further factors κ, κ^2, in the context of §6*b*, and a derivative (multiplied by a pure imaginary constant) operates on the left-hand side of (6.28*c*), although no significant change is produced in the ultimate behaviour described earlier in this section. The author thanks Dr R. G. Bowles and Mr B. T. Dodia, with whom further research is being conducted. Support from SERC, U.K., from Ohio State University in the form of a Distinguished Visiting Professorship during part of this research, and from AFOSR (grant no. 89-0475), is gratefully acknowledged.

Appendix A. Some coefficients appearing in §3

The coefficients $\chi_{-1}, \chi_L, \hat{\chi}_{-1}$ appearing in (3.12*a*, *b*), and certain coefficients in (3.15*a*–*c*), are defined as follows.

PHILOSOPHICAL TRANSACTIONS OF THE ROYAL SOCIETY A MATHEMATICAL, PHYSICAL & ENGINEERING SCIENCES

First, directly from the momentum equations,

$$\chi_{-1\eta} = \mu^{-2}(-\beta_1 b_1^{-1} + \beta_2 b_1^{-2} - \beta_3 b_1^{-3}), \tag{A 1}$$

so that on integration

$$\chi_{-1} = kBb_1^{-1}\mu^{-2}|g_0|^2. \tag{A 2}$$

Also, $\hat{\chi}_{-1} = \mu\chi_{-1}$, and

$$\chi_L = -2Bkb_1^{-2}\mu^{-1}(\lambda + \mu^{-1}B), \tag{A 3}$$

from working similar to that in (A 1), (A 2).

Second, the relations

$$b_1\kappa_{-1} = B(k+2)\,g_0\chi_{-1}, \tag{A 4}$$

$$-b_1\kappa_L - B\kappa_{-1} = \lambda^2 b_1^{-2}(\lambda\hat{\chi}_{-1} + B\chi_{-1}) + \lambda\kappa Bb_1^{-1}g_0\hat{\chi}_{-1} - B^2b_1^{-1}g_0\chi_L, \tag{A 5}$$

$$b_1\tilde{\kappa}_{-1} = \lambda b_1^{-1}g_0(\lambda\hat{\chi}_{-1} + B\chi_{-1}) + kBg_0\hat{\chi}_{-1}, \tag{A 6}$$

$$\hat{\kappa}_L = \mathrm{i}b_1^{-1}B^2g_0\chi_L \tag{A 7}$$

determine the coefficients $\kappa_{-1}, \kappa_L, \tilde{\kappa}_{-1}, \hat{\kappa}_L$ in turn.

Appendix B. The main details for case II, in §6*b*

With (6.27) holding, the expansions in (3.1*a–e*) yield the following main properties.

First, the continuity balances stay as in (3.2*a–f*), except that now

$$u_{10} = A_{10}, \quad v_{20} = \mu A_{10\eta}\,s, \tag{B 1}$$

and v_{10} is identically zero again, so that the subscripts 10, 20 in (3.2*f*) are replaced by 20, 30 respectively.

Second, in the streamwise momentum balances (3.3*a–f*), the only remaining term now among the nonlinear ones on the left-hand side in (3.3*e*) is

$$\mathrm{i}BA_{10}\,u_0, \tag{B 2}$$

and the change of subscripts described just after (B 1) applies to the left-hand side of (3.3*f*). Otherwise, (3.3*a–f*) remain intact, as does the formula for f_1 in (3.3*g*).

Third, corresponding changes occur in the spanwise momentum balances of (3.4*a–f*), with the nonlinearity on the left-hand side of (3.4*e*) being due solely to a term

$$\mathrm{i}BA_{10}\,w_0, \tag{B 3}$$

while w_{10} in (3.4*f*) is replaced by w_{20}. The function f_2 remains as in (3.4*g*).

As a result of the above modifications, the nonlinear influences due to the second-harmonic terms such as $u_0 u_{12}$ are reduced to higher-order effects, and so the second-harmonic equations (3.2*b*), (3.3*b*), (3.4*b*) become redundant as regards the rest of the working below leading to the amplitude equation. The fundamental solutions are still given by (3.5)–(3.6*e*), (3.8*a–d*). Hence for the spanwise mean-flow correction in (3.4*f*), modified as above, the tangential-flow condition as $s \to 0+$ yields the requirement that

$$g_{10\eta} = -f_2 \quad \text{at} \quad s = 0, \tag{B 4}$$

because the mean flow is now much weaker near the surface than that in case I in §3. Use of (3.4*g*) for f_2, followed by integration with respect to η, then leads to the result (6.28*a*), after some manipulation. Exactly the same result is found from setting v_{30} and s to zero in the modified version of (3.3*f*), on use of (3.3*g*) for f_1.

The result (6.28*b*), on the other hand, stems from the external pressure expansion, which is now of the form (6.1) but with κ^N powers inserted as in (3.1*d*) and with κ

given by (6.27). Since the external relations are all linear, however, and the appearances of powers of κ in (3.1d, e) are identical apart from the new $\hat{X}^{\frac{2}{3}}$ shift associated with g_{10}, A_{10}, the result (6.28b) is implied directly by (6.11).

Finally here, the forced fundamentals w_{21}, u_{21} are analogous with (3.13a, b) except that the contributions due to second harmonics must be omitted now. The displacement effect in (B 1) for instance gives terms $-\delta^{-1}BA_{10}w_0$, $-\delta^{-2}\lambda^2 A_{10}g_0$ in w_{21}, u_{21} in turn. The subsequent internal pressure–displacement relation obtained from letting $s \to 0+$ is therefore the corresponding analogue of (6.16). The external relation remains exactly as in (6.10), and so the coupling of the internal and external relations produces the result quoted in (6.28c).

Appendix C. Computational solutions for case II

The governing equations (6.30a, b) for case II were treated numerically by a finite-difference procedure. This was designed to allow for the growth

$$\bar{A} \sim h_1 \hat{\eta}^{\frac{1}{2}} \quad \text{as} \quad \hat{\eta} \to +\infty, \tag{C 1}$$

where h_1 is a positive constant. The growth (C 1) is implied by (6.30b), given that (6.30a) yields the asymptote

$$g \propto |\hat{\eta}|^{-\frac{1}{4}} \sin\{\tfrac{2}{3}|\hat{\eta}|^{\frac{3}{2}} + \text{const.}\} \quad \text{as} \quad \hat{\eta} \to -\infty \tag{C 2}$$

since $|\bar{A}| \ll |\hat{\eta}|^{\frac{1}{2}}$ at large negative $\hat{\eta}$, whereas $\hat{g}$ decays exponentially as $\hat{\eta} \to +\infty$. We note in passing that (C 1) indicates the presence of a significant negative mean-flow displacement persisting outside the wing-tips of the spot.

In view of (C 1), we worked in terms of the derivative function

$$\bar{B} = \bar{A}'(\hat{\eta}), \tag{C 3}$$

replacing (6.30b) by

$$-2\pi g g' = \int_{-\infty}^{\infty} \frac{\bar{B}'(\xi)\,\mathrm{d}\xi}{(\hat{\eta}-\xi)}, \tag{C 4}$$

coupled with (6.30a). Here (C 3), (C 4) are discretized in the forms

$$\tfrac{1}{2}(\bar{B}_i + \bar{B}_{i-1}) = (\bar{A}_i - \bar{A}_{i-1})/\Delta\hat{\eta}, \tag{C 5}$$

$$(-\pi/\Delta\hat{\eta})\,(g_i^2 - g_{i-1}^2) = \nu_1 + \nu_2 \bar{B}_i \tag{C 6}$$

in a standard notation, where

$$\nu_1 = -(\Delta\hat{\eta})^{-1} \sum_{j \neq i} \{(i-j)^2 - \tfrac{1}{4}\}^{-1} B_j \tag{C 7}$$

and $\nu_2 = 4(\Delta\hat{\eta})^{-1}$; see Davis & Werle (1982). The $\hat{\eta}$ variable is given by $\hat{\eta}_{-\infty} + (i-1)\,\Delta\hat{\eta} = \hat{\eta}_i$, with $1 \leqslant i \leqslant I$, $\hat{\eta}_\infty = \hat{\eta}_{-\infty} + (I-1)\,\Delta\hat{\eta}$, and $\hat{\eta}_{\pm\infty}$ are chosen to be suitably large, with the step size $\Delta\hat{\eta}$ being small. The corresponding discretization taken for (6.30a) is

$$\frac{(g_{i+1} - 2g_i + g_{i-1})}{(\Delta\hat{\eta})^2} - \hat{\eta}_i g_i = -\bar{A}_i g_i. \tag{C 8}$$

The system (C 5)–(C 8) is then solved by a Newton iteration scheme based on substituting from (C 5), (C 6) into (C 8), to produce a nonlinear equation for g_i in terms of function values at steps other than i, and inversion of a tridiagonal system for the gs. All the $\bar{A}_i, \bar{B}_i$ values for $1 \leqslant i \leqslant I$ are then updated from (C 5), (C 6), the

iteration scheme is continued as above, and so on. Use of the derivative function $\bar{B}$ to accommodate the growth (C 1) proved very advantageous for obtaining accuracy, at least compared with using $\bar{A}, g$ alone.

The procedure appeared to work reasonably well, its typical converged results being shown in figure 3. Tests on the grid effects present through $\hat{\eta}_{\pm\infty}$ and $\Delta\hat{\eta}$ were conducted and proved fairly affirmative, the typical grid distribution with $\hat{\eta}_{-\infty} = -100$, $\hat{\eta}_{+\infty} = 100$, $\Delta\hat{\eta} = 0.1$ giving satisfactory accuracy in most cases.

Appendix D. The behaviour of solutions for case II at large amplitudes

It is proposed here that at large amplitudes the solution of (6.30*a*, *b*) for case II becomes multistructured, with three dominant regions present separated by two relatively thin adjustment regions. This structure is suggested partly by the computational results in figure 3 and Appendix C but more so by its self-consistency. We note in addition that descriptions based on a single dominant region or on two such regions separated by one adjustment region were tried first in this research but they appeared to yield contradictions in part of the solution domain. The three-plus-two description which apparently works is as follows.

The left-hand region (L) extends to $\hat{\eta} = -\infty$ and has

$$g = \bar{g}(\eta^*) + \ldots, \quad \hat{\eta} = \Delta\bar{\eta}, \quad \hat{\eta} = \Delta^{-\frac{1}{2}}\eta^*, \tag{D 1}$$

$$\bar{A} = \Delta\bar{a}(\bar{\eta}) + \ldots, \quad \text{with} \quad \Delta \gg 1, \tag{D 2}$$

and $\bar{A} > \bar{\eta}$, so that $\bar{a} > \bar{\eta}$. Here the slow variable $\bar{\eta}$ runs from $-\sigma$ to $-\infty$, where σ is a finite constant, while η^* is the fast variable giving the main dependence of $\bar{g}$ but only a higher-order effect in $\bar{A}$, as we see below. Substitution into (6.30*a*) leaves $\bar{g}$ controlled by

$$\mathrm{d}^2\bar{g}/\mathrm{d}\eta^{*2} = (\bar{\eta} - \bar{a})\,\bar{g}, \tag{D 3}$$

and similarly for further terms in the expansion, so that the $\bar{g}$ solution is highly oscillatory,

$$\bar{g} = (\bar{a} - \bar{\eta})^{-\frac{1}{4}} k_1 \cos\left[\int (\bar{a} - \bar{\eta})^{\frac{1}{2}} \mathrm{d}\eta^* + k_2\right] \tag{D 4}$$

formally. In (D 4) the expression for the coefficient of the cosine follows from terms of higher order, and k_1, k_2 are constants, the first of which may be taken to be unity by suitably defining Δ above. Turning to (6.30*b*), therefore, we find that the latter's left-hand side ($-g^2$) has both slow and fast dependences present, from (D 4), but the slow part dominates in the determination of $\bar{a}(\bar{\eta})$ because of the integral nature of the right-hand side. Thus, if for convenience the left-hand side is regarded as an effective pressure, $\bar{P}$ say, then we have the conditions

$$\left.\begin{aligned} &\bar{P} = -\tfrac{1}{2}(\bar{a} - \bar{\eta})^{-\frac{1}{2}}, && (\text{D 5}) \\ &\bar{a}\,(> \bar{\eta}) \text{ is unknown}, && (\text{D 6}) \end{aligned}\right\} \quad \text{for} \quad \bar{\eta} < -\sigma,$$

so far, to be tied in with (6.30*b*).

The middle region (M) covers a finite range of $\bar{\eta}$, $-\sigma < \bar{\eta} < \kappa$ say, where $\kappa(> -\sigma)$ is an $O(1)$ constant. Here the variation of the solution is slower, with

$$g = \bar{g}(\bar{\eta}) + \ldots, \tag{D 7}$$

$$\bar{A} = \Delta\bar{\eta} + \Delta^{-2}\bar{A}_1(\bar{\eta}) + \ldots, \tag{D 8}$$

the slower variation being due to the near-equality of $\bar{A}, \hat{\eta}$. From (6.30a), $\bar{g}, \bar{A}_1$ are interrelated by

$$\bar{g}_{\bar{\eta}\bar{\eta}} = -\bar{A}_1 \bar{g}, \tag{D 9}$$

which serves to determine the correction term in (D 8) once $\bar{g}(\bar{\eta})$ is found (from below). So the dominant result here as regards solving (6.30a, b) is that

$$\left.\begin{aligned} &\bar{P}\,(<0) \text{ is unknown,} \\ &\bar{a} \equiv \bar{\eta}, \end{aligned}\right\} \quad \text{for} \quad -\sigma < \bar{\eta} < \kappa, \tag{D 10, D 11}$$

the latter following from (D 8), cf. (D 2).

The right-hand region (R), extending from $\Delta\kappa$ to $+\infty$, has $\bar{A}$ as in (D 2) effectively but now $\bar{a}(\bar{\eta}) < \bar{\eta}$. Hence the counterpart of (D 3) demands that $\bar{g}$ be exponentially small. This provides the conditions

$$\left.\begin{aligned} &\bar{P} \equiv 0, \\ &\bar{a}\,(<\bar{\eta}) \text{ is unknown,} \end{aligned}\right\} \quad \text{for} \quad \bar{\eta} > \kappa, \tag{D 12, D 13}$$

on the relation (6.30b).

The task, then, is to solve (6.30b), or rather the integral equation

$$\bar{P}(\bar{\eta}) = \frac{1}{\pi} \int_{-\infty}^{\infty} \frac{\bar{a}'(\xi)\,\mathrm{d}\xi}{(\bar{\eta}-\xi)}, \tag{D 14}$$

subject to the mixed constraints (D 5), (D 6), (D 10), (D 11), (D 12), (D 13) for the three dominant regions. This may be done as in Mushkileshvili (1953) (see also Carrier *et al.* 1966), or by considering the function

$$(\bar{Z}-\kappa)^{-\frac{1}{2}}(\bar{Z}+\sigma)^{\frac{1}{2}}(\bar{P}-\mathrm{i}\bar{a}') \tag{D 15}$$

extended into the complex plane ($\bar{Z} = \bar{\eta} + \mathrm{i}\bar{Y}$ say). In consequence we obtain, after some manipulation, the single-region integral equation

$$\frac{2Q'}{Q^3} = \frac{(\kappa-\bar{\eta})^{\frac{1}{2}}}{(-\sigma-\bar{\eta})^{\frac{1}{2}}}\left[1 - \frac{1}{2\pi}\int_{-\infty}^{-\sigma} \frac{(-\sigma-\xi)^{\frac{1}{2}} Q(\xi)\,\mathrm{d}\xi}{(\kappa-\xi)^{\frac{1}{2}}(\bar{\eta}-\xi)}\right], \tag{D 16}$$

for the function $Q(\bar{\eta})$ in the range $\bar{\eta} < -\sigma$, where the substitution $\bar{a} = \bar{\eta} + Q^{-2}$ has been made in that range and $Q\,(= -2\bar{P})$ is required to be positive. A useful alternative to (D 16) is the equation

$$\frac{2Q'}{Q^3} = \frac{(-\sigma-\bar{\eta})^{\frac{1}{2}}}{(\kappa-\bar{\eta})^{\frac{1}{2}}}\left[1 - \frac{1}{2\pi}\int_{-\infty}^{-\sigma} \frac{(\kappa-\xi)^{\frac{1}{2}} Q(\xi)\,\mathrm{d}\xi}{(-\sigma-\xi)^{\frac{1}{2}}(\bar{\eta}-\xi)}\right] + \left(\frac{D}{2\pi} - 1\right)(\kappa+\sigma)\,(-\sigma-\bar{\eta})^{-\frac{1}{2}}(\kappa-\bar{\eta})^{-\frac{1}{2}}, \tag{D 17}$$

where the constant

$$D = \int_{-\infty}^{-\sigma} \frac{Q(\xi)\,\mathrm{d}\xi}{(-\sigma-\xi)^{\frac{1}{2}}(\kappa-\xi)^{\frac{1}{2}}}, \tag{D 18}$$

which may be used to verify some of the properties given below.

The relations (D 16), (D 17) are consistent with the following features of the solution near the junctions $\bar{\eta} = -\sigma$, $\bar{\eta} = \kappa$, and as $\eta \to \pm\infty$. First,

$$\bar{P} \sim -\alpha_1(-\sigma-\bar{\eta})^{-\frac{1}{4}}, \quad \bar{a} \sim -\sigma + 4\alpha_1^{-2}(-\sigma-\bar{\eta})^{\frac{1}{2}} \quad \text{as} \quad \bar{\eta} \to -\sigma(-), \tag{D 19}$$

where, provided $D < 2\pi$,

$$\sigma_1 = 2^{-\frac{3}{2}}(\kappa+\sigma)^{-\frac{1}{4}}(1-D/2\pi)^{-\frac{1}{2}}.$$

Second, from the analogue of (D 16), (D 17) applied in the middle region M,

$$\bar{P} \sim -\alpha_2(\sigma+\bar{\eta})^{-\frac{1}{2}} \quad \text{as} \quad \bar{\eta} \to -\sigma(+), \tag{D 20}$$

$$\bar{P} \sim -\alpha_3(\kappa-\bar{\eta})^{\frac{1}{2}} \quad \text{as} \quad \bar{\eta} \to \kappa(-), \tag{D 21}$$

where $\alpha_2 = (\kappa+\sigma)^{\frac{1}{2}}(1-D/2\pi)$,

$$\alpha_3 = (\sigma+\kappa)^{-\frac{1}{2}}\left[1-\frac{1}{2\pi}\int_{-\infty}^{-\sigma}\frac{(-\sigma-\xi)^{\frac{1}{2}}Q(\xi)\,\mathrm{d}x}{(\kappa-\xi)^{\frac{3}{2}}}\right].$$

Third, the analogue for the right-hand region R gives

$$\bar{a} \sim \kappa+(\bar{\eta}-\kappa)-\tfrac{2}{3}\alpha_3(\bar{\eta}-\kappa)^{\frac{3}{2}} \quad \text{as} \quad \bar{\eta} \to \kappa(+). \tag{D 22}$$

In the above the constants $\alpha_1, \alpha_2, \alpha_3$ are all positive, and the conditions associated with (D 5), (D 6), (D 10)–(D 13) are all satisfied locally, as a check. The appearance of $\frac{1}{2}$ powers (etc.) locally is to be expected. Fourth, we find that

$$\bar{a} \sim \alpha_4\bar{\eta}^{\frac{1}{2}} \quad \text{as} \quad \bar{\eta} \to \infty, \tag{D 23}$$

$$\bar{P} \sim -\tfrac{1}{2}\alpha_4|\bar{\eta}|^{-\frac{1}{2}} \quad \text{as} \quad \bar{\eta} \to -\infty, \tag{D 24}$$

with the constant α_4 being equal to unity and the responses (D 23), (D 24) are in line with that of (C 1). The corresponding behaviours for Q, in the left-hand region L, follow from the above as

$$Q \sim \begin{cases} 2\alpha_1(-\sigma-\bar{\eta})^{-\frac{1}{4}} & \text{as} \quad \bar{\eta} \to -\sigma(+), \\ |\bar{\eta}|^{-\frac{1}{2}} & \text{as} \quad \bar{\eta} \to -\infty, \end{cases} \tag{D 25}$$

and these are used below.

Again, closer to the junctions there are thin adjustment zones. Near $\bar{\eta} = -\sigma$, the adjustment zone has

$$g = \Delta^{\frac{3}{10}}g_1(\eta_1)+\ldots, \quad \hat{\eta} = -\Delta\sigma+\Delta^{-\frac{1}{5}}\eta_1, \quad \bar{A} = -\Delta\sigma+\Delta^{\frac{2}{5}}A_1(\eta_1)+\ldots \tag{D 26}$$

and, from (6.30a, b), the local governing equations are

$$g_1'' = -A_1 g_1, \quad -g_1^2 = \frac{1}{\pi}\int_{-\infty}^{\infty}\frac{A_1'(\xi)\,\mathrm{d}\xi}{(\eta_1-\xi)}, \tag{D 27}$$

along with the matching conditions

$$|g_1| \ll |\eta_1|^{-\frac{1}{4}}, \quad |A_1| \sim 4\alpha_1^{-2}|\eta_1|^{\frac{1}{2}}, \quad \text{as} \quad \eta_1 \to -\infty, \tag{D 28}$$

$$g_1 \sim (2\alpha_2)^{\frac{1}{2}}\eta_1^{-\frac{1}{4}}, \quad |A_1| \ll \eta_1^{\frac{1}{2}}, \quad \text{as} \quad \eta_1 \to \infty, \tag{D 29}$$

due to the L- and M-region properties above. The adjustment zone close to $\bar{\eta} = \kappa$, on the other hand, has

$$g = \Delta^{-\frac{3}{14}}g_2(\eta_2)+\ldots, \quad \hat{\eta} = \Delta\kappa+\Delta^{\frac{1}{7}}\eta_2, \quad \bar{A} = \Delta\kappa+\Delta^{\frac{1}{7}}\eta_2+\Delta^{-\frac{2}{7}}A_2+\ldots, \tag{D 30}$$

as implied by the M- and R-region behaviours nearby. Here (6.30a, b) yield the controlling equations

$$g_2'' = -A_2 g_2, \quad -g_2^2 = \frac{1}{\pi}\int_{-\infty}^{\infty}\frac{A_2'(\xi)\,\mathrm{d}\xi}{(\eta_2-\xi)}, \tag{D 31}$$

similar to those in (D 27), but subject to the matching constraints

$$g_2 \sim \alpha_3^{\frac{1}{2}}|\eta_2|^{\frac{1}{2}}, \quad |A_2| \ll |\eta_2|^{\frac{3}{2}}, \quad \text{as} \quad \eta_2 \to -\infty, \tag{D 32}$$

$$g_2 \ll \eta_2^{\frac{1}{2}}, \quad A_2 \sim -\tfrac{2}{3}\alpha_3 \eta_2^{\frac{3}{2}} \quad \text{as} \quad \eta_2 \to \infty, \tag{D 33}$$

in view of the solutions in the M and R regions locally: see (D 21), (D 22).

The first priority, however, is to solve (D 16) subject to (D 25). This was done numerically using a finite-difference scheme, but applied to

$$\tilde{Q} \equiv (\kappa+\sigma)^{\frac{1}{3}}(-\sigma-\bar{\eta})^{\frac{1}{3}}(\kappa-\bar{\eta})^{-\frac{1}{2}}Q$$

regarded as a function of $(\bar{\eta}+\sigma)(\kappa+\sigma)^{-1}$. The latter step is for normalization purposes, since then, in (D 16), σ, κ are replaced by $0, 1$ in turn and a factor $(\kappa+\sigma)^{\frac{1}{3}}$ is added, in effect. The scheme is used on the $\bar{\eta}$-derivative of (D 16), to compensate for the factor just mentioned, with zero conditions on $\tilde{Q}$ corresponding to (D 25) being imposed in principle at the ends $-\infty, 0$; in fact asymptotic decay conditions were imposed on $\tilde{Q}$ at a large negative value and a small negative value of $\bar{\eta}$, respectively. The scheme treats the Cauchy–Hilbert integral involved as in Appendix C, the other terms are written in a centred-difference form, and an iterative multi-sweeping method is adopted to handle the elipticity and nonlinearity present. The results are shown in figure 4, and they have been tested for grid-distribution effects, which were found to be very small for a typical grid of 1001×0.02 points in $|\bar{\eta}|$ normalized as above. In addition, the behaviours predicted analytically in (D 25), and earlier in (D 19), (D 24), appear to be verified well in the computational results; and there is fair agreement with the trends of the full results of Appendix C, figure 3, at increasing amplitude.

References

Bandyopadhyay, P. R. 1983 In *Proc. Fourth Int. Conf. Physicochem. Hydrod.*, pp. 393–395. Annals of the New York Academy of Sciences.

Benny, D. J. & Bergeron, R. F. 1969 *Stud. appl. Math.* **48**, 181–204.

Bodonyi, R. J., Gajjar, J. S. B. & Smith, F. T. 1983 *IMA J. appl. Math.* **30**, 1–19.

Bullister, E. T. & Orszag, S. A. 1987 *J. Sci. Comput.* **2**, 263–281.

Carrier, G. F., Krook, M. & Pearson, C. E. 1966 *Functions of a complex variable.* McGraw-Hill.

Cates, A. T. & Crighton, D. G. 1990 *Proc. R. Soc. Lond.* A **430**, 69–88.

Chambers, F. W. & Thomas, A. S. W. 1983 *Phys. Fluids* **26**, 1160–1162.

Davis, R. T. & Werle, M. J. 1982 In *Numerical and physical aspects of aerodynamic flows* (ed. T. Cebeci). Springer.

Doorly, D. J. & Smith, F. T. 1992 Initial-value problems for spot disturbances in incompressible or compressible boundary layers. *J. Engng Math.* **26**, 87–106.

Emmons, H. W. 1951 *J. aeronaut. Sci.* **18**, 490–498. (See also *J. Fluid Mech.* **9**, 235–246 (1963).)

Falco, R. E. 1979 In *Proc. Sixth Biennial Symp. Turb.* (ed. X. X. Zakin & Y. Y. Patterson), ch. 1.1–1.4. University of Missouri-Rolla.

Fasel, H. 1990 In *Laminar-turbulent transition* (ed. D. Arnal & R. Michel). Berlin: Springer-Verlag.

Fasel, H. & Konzelmann, U. 1991 In *Proc. R. aeronaut. Soc. Meeting on Transition.* Cambridge, U.K.

Gad-el-Hak, M., Blackwelder, R. F. & Riley, J. J. 1981 *J. Fluid Mech.* **110**, 73–95.

Gaster, M. 1968 *J. Fluid Mech.* **32**, 173–184.

Gaster, M. 1990 *Proc. R. Soc. Lond.* A **430**, 3–24.

Glezer, A., Katz, Y. & Wygnanski, I. J. 1989 *J. Fluid Mech.* **198**, 1–26.

Haberman, R. 1972 *Stud. appl. Math.* **51**, 139–161.

PHILOSOPHICAL TRANSACTIONS OF THE ROYAL SOCIETY A MATHEMATICAL, PHYSICAL & ENGINEERING SCIENCES

Hall, P. & Smith, F. T. 1991 *J. Fluid Mech.* **227**, 641–666.

Head, M. R. & Bandyopadhyay, P. 1981 *J. Fluid Mech.* **107**, 297–338.

Henningson, D. S. & Alfredson, P. H. 1987 *J. Fluid Mech.* **178**, 405–421.

Henningson, D. S., Spalart, P. & Kim, J. 1987 *Phys. Fluids* **30**, 2914–2917.

Henningson, D. S. & Kim, J. 1991 *J. Fluid Mech.* **228**, 183–205.

Howe, M. S. 1967 *J. Fluid Mech.* **30**, 497–512.

Howe, M. S. 1988 *J. Fluid Mech.* **32**, 779–789.

Hoyle, J. M., Smith, F. T. & Walker, J. D. A. 1991 *Comp. Phys. Communs* **65**, 151–157. (See also *Proc. IMACS Conf.*, 1990, Boulder, Colorado, U.S.A.)

Hunter, J. K. & Keller, J. B. 1988 *Proc. R. Soc. Lond.* A **417**, 299–308.

Johansson, A. V., Her, J. Y. & Haritonidis, J. H. 1987 *J. Fluid Mech.* **175**, 119–142.

Katz, Y., Seifert, A. & Wygnanski, I. 1990 *J. Fluid Mech.* **221**, 1–22.

Leonard, A. 1981 *Lect. Notes Phys.* **136**, 11145, Springer-Verlag, Berlin.

Lighthill, M. J. 1963 *Laminar boundary layers* (ed. L. Rosenhead), ch. II. Oxford University Press.

Miles, J. W. 1978 *Proc. R. Soc. Lond.* A **361**, 277–291.

Mushkileshvili, N. I. 1953 *Singular integral equations*. Gronigen, The Netherlands: Nordhoff.

Peridier, V. J., Smith, F. T. & Walker, J. D. A. 1991*a* *J. Fluid Mech.* **232**, 99–131.

Peridier, V. J., Smith, F. T. & Walker, J. D. A. 1991*b* *J. Fluid Mech.* **232**, 133–165.

Perry, A. E., Liu, T. T. & Teh, E. W. 1981 *J. Fluid Mech.* **104**, 387–405.

Riley, J. J. & Gad-el-Hak, M. 1985 In *Frontiers in Fluid Mechanics* (ed. S. H. Davies & J. L. Lumley), pp. 123–155. New York: Springer-Verlag.

Robinson, S. K. 1991 *Rev. Fluid Mech.* **23**, 601–639.

Rosales, R. R. 1978 *Proc. R. Soc. Lond.* A **361**, 265–275.

Schlichting, H. 1979 *Boundary-layer theory*, 4th edn. McGraw-Hill.

Schubauer, G. B. & Klebanoff, P. S. 1956 *NACA Rep.* 1289.

Smith, C. R., Walker, J. D. A., Haidari, A. H. & Sobrun, U. 1991 *Phil. Trans. R. Soc. Lond.* A **336**, 131–175.

Smith, F. T. 1988 *Mathematika* **35**, 256–273.

Smith, F. T. 1991*a* *Computers Fluids* **20**, 243–268. (Also given as a presentation at the R. T. Davis Memorial Symp., Cincinnati, U.S.A. (1987).)

Smith, F. T. 1991*b* AIAA paper no. 91-0331. (Also *AIAA J.* (In the press.).)

Smith, F. T. 1992 In preparation.

Smith, F. T. & Bodonyi, R. J. 1982 *J. Fluid Mech.* **118**, 165–185.

Smith, F. T. & Burggraf, O. R. 1985 *Proc. R. Soc. Lond.* A **399**, 25–55.

Smith, F. T., Doorly, D. J. & Rothmayer, A. P. 1990 *Proc. R. Soc. Lond.* A **428**, 255–281.

Stuart, J. T. & Tabor, M. 1990 *Phil. Trans. R. Soc. Lond.* A **333**, 263–271.

Walker, J. D. A. 1990 In *Proc. Second IUTAM Symp. on structure of turbulence and drag reduction* (ed. A. Gyr), pp. 109–117. New York: Springer.

Wygnanski, I. J., Haritonides, J. H. & Kaplan, R. E. 1979 *J. Fluid Mech.* **92**, 505.

Received 23 September 1991; accepted 18 November 1991

PHILOSOPHICAL TRANSACTIONS OF THE ROYAL SOCIETY A MATHEMATICAL, PHYSICAL & ENGINEERING SCIENCES